Int J Environ Res (2024) 18:3
https://doi.org/10.1007/s41742-023-00554-6

REVIEW ARTICLE

# Carbon-Based Catalysts for Clean Environmental Remediation

**Ajit Dattatray Phule[1,2] · Md. Wahad Uz Zaman[1] · Sahar Elkaee[1] · Seul Yi Kim[1] · Sang Gyu Lee[1] · Gibeom Park[1] · Jae Hwan Yang[1,2]**

Received: 3 August 2023 / Revised: 26 September 2023 / Accepted: 5 November 2023 / Published online: 6 December 2023


## Abstract

Air pollution, owing to gaseous pollutants, especially NOx, VOCs (toluene), acidic gas ($H_2S$), and elemental mercury ($Hg^0$), and the resulting climate issues have become major concerns. Carbon-based catalysts play a key role in removing toxic gases through selective catalytic reduction (SCR), oxidation, and adsorption processes. Catalyst selection has a crucial effect on the final toxic gas removal performance of catalyst. Herein, strategies for modifying carbon-based catalysts through physical or chemical treatment/activation, metal oxide doping, and heteroatom doping are systematically reviewed. In addition, the effects of the carbonization temperature, pore structure, heteroatom dopants, and oxidizing agents on the surface area, pore structure, and catalytic effects of carbon-based catalysts are analyzed and discussed. Finally, the further direction and need for developing carbon-based catalysts for environmental remediation is prospected.

## Highlights

- **Carbon-based catalysts for environmental remediation are discussed.**
- **Modification strategies for carbon-based catalysts are provided in detail.**
- **Various air pollutant-removal performances of the modified catalyst are briefed.**
- **Challenges and future prospects of carbon catalysts are presented.**

**Keywords** Porous carbon catalyst · Air pollution · Heteroatom doping · Metal oxides · Carbonization · Porous structure

## Abbreviations

| | |
|---|---|
| AC | Activated catalyst |
| C/SAC-2 | Chemically activated catalyst |
| Co/SAC-2 | Co-activated catalyst |
| NOAC | N- and O-doped AC |
| NHPC | N-doped hierarchical porous carbon |
| NPC | N-doped porous carbon |
| NSDG-10 | N- and S-doped nanoporous carbon |
| $PBC_{900}$ | P-doped biochar |
| PAN | Polyacrylonitrile |
| P/SAC | Physically activated catalyst |
| SAC | *Sargassum*-Based carbon |
| SCR | Selective catalytic reduction |
| SMC-900 | S-doped mesoporous carbon |
| SSA | Specific surface area |
| WS | Wheat straw |
| NG | Nitrogen doped graphene |
| ORR | Oxygen reductive reaction |

✉ Jae Hwan Yang
yjh98@cnu.ac.kr

[1] Department of Environmental Engineering, Chungnam National University, 99 Daehak-Ro, Yuseong-Gu, Daejeon 34134, South Korea

[2] Department of Environmental and IT Engineering, Chungnam National University, 99 Daehak-Ro, Yuseong-Gu, Daejeon 34134, South Korea

## Introduction

Although industrialization has improved the quality of life of everyone, it has also created a huge problem of air pollution—a major global health and environmental challenge. The chief sources of toxic gases are industries (coal power plants, refineries, and petrochemicals), coal combustion, mining of mineral resources, transportation (land, water, and air), landfills, and waste management (Damma et al. 2019; Li et al. 2022c; Wang et al. 2014; Zhang et al. 2017). Many methods have been developed for controlling air pollution,

including selective catalytic reduction (SCR), oxidation, adsorption, and photochemical treatments (Ahmadi et al. 2021; Li et al. 2023a, c; Zhou et al. 2019). The catalysts used in such remediation methods typically have an active site with a support/carrier to facilitate the mineralization of toxic gases. Metal oxide-based catalysts are excellent commercial candidates for removing toxic gases through SCR, oxidation, and adsorption (Anthonysamy et al. 2018; Kim et al. 2018; Murindababisha et al. 2021). However, their narrow operating window, toxicity, high cost, and thermal instability limit their applicability. Hence, such catalysts need to be further improved.

Porous carbon catalysts have shown great potential for environmental remediation due to their distinctive properties such as a high specific surface area, a distinct structure, tunable porosity, and excellent chemical stability (Chiang et al. 2001; Gao et al. 2019; Tian et al. 2001). These carbon catalysts are commonly used in various applications, including for removing pollutants from air and water, for degrading organic compounds, photocatalytic degradation activity, and for electrocatalysis (especially carbon-based single atom catalyst) (Bai et al. 2023a, b; Guo et al. 2020; Gupta and Saleh 2013; Jin et al. 2022b; Li et al. 2015b; Pan et al. 2022; Shi et al. 2021; Shi et al. 2022b, c; Shi et al. 2023; Tang et al. 2022, 2023a, b, c; Wang et al. 2023b; Zhang et al. 2017). Porous carbon materials can also be sintered as active support materials. Several methods that use porous carbon materials have been modified to improve the catalytic performance of such materials (Anthonysamy et al. 2018). A porous carbon-based catalyst with good adsorption properties and a good support/carrier is a crucial component of catalytic systems for removing toxic gases (Cho et al. 2023). However, the insufficient activity of carbon materials, inadequate waste recycling, and poor high-temperature stability need to be effectively addressed before porous carbon-based catalysts could be used for removing pollutants.

This review summarizes the progress made so far in developing porous carbon material-based catalysts for achieving clean environmental remediation. Although several review papers have dealt with carbon-based materials for applications of various catalytic reactions, it still lacks the systematic study that delves into the utilization of carbon-based catalysts for the clean air environments. The current review mainly focuses on the methods developed for removing major toxic gases such as $NO_x$, VOCs (such as toluene), acidic gases (such as $H_2S$), and elemental mercury ($Hg^0$). It also discusses the modification strategies for the development of porous carbon with physical or chemical treatments, metal oxide doping, and heteroatom doping, as well as the effects of various physicochemical parameters on reducing the release of the above mentioned toxic gases (Fig. 1). Finally, future perspectives and possible directions are presented.

## Strategies for Fabricating Modified Carbon-Based Catalysts for Removing Air Pollutants

Carbon as a support material plays a vital role in heterogeneous catalysis because of its superior physical and chemical properties compared to those of other supports (Fidalgo and Menéndez 2011). Support materials with a high surface area, suitable chemical composition, and porous structure can accommodate catalytic species/active phases to improve the activity or selectivity of the corresponding catalyst, which can also influence the dispersion and accessibility of catalytic species on the surface of carbon support materials. Catalysts can be further modified by physicochemical treatments, using metal oxides, and through heteroatom (N, O, and S/P, B) doping to improve their activity.

## Modification of Carbon Support Materials

### Physical or Chemical Treatment/Activation

The aim of activation, which involves physical or chemical treatment, is to improve the porosity, pore volume, and surface area of carbon materials. Activation through physical treatments mainly involves thermal treatment (pyrolysis or carbonization) at high temperatures through steam or gas purging (using gases such as $CO_2$, steam, and $N_2$). The oxidation of the carbon source material at high temperatures (i.e., the conversion of surface carbon and hydrogen into $CO_2$ and $H_2O$, respectively) changes the surface area and porosity in a controlled way (Li et al. 2015b; Panwar and Pawar 2022). $CO_2$ activation forms micropores, while steam activation increases their size. Chemical treatments commonly employ chemical agents [such as KOH, NaOH, $H_3PO_4$, $H_2SO_4$, and $(NH_4)_2SO_4$] in one- or two-step processes. These treatments improve the surface area and pore structure of the catalyst and increase its surface oxygen functional moieties (Ku et al. 1994). In a one-step process, the carbonization and activation of the precursor material can be achieved simultaneously by using a chemical agent (Li et al. 2015b). In contrast, the two-step process involves carbonization, followed by activation using chemical agents or pretreatment of the precursor material with a chemical agent before carbonization (Guo et al. 2007).

### Metal Oxide Doping

Carbon materials can be modified by doping with metal oxides (mostly transition metal oxides) that improves the

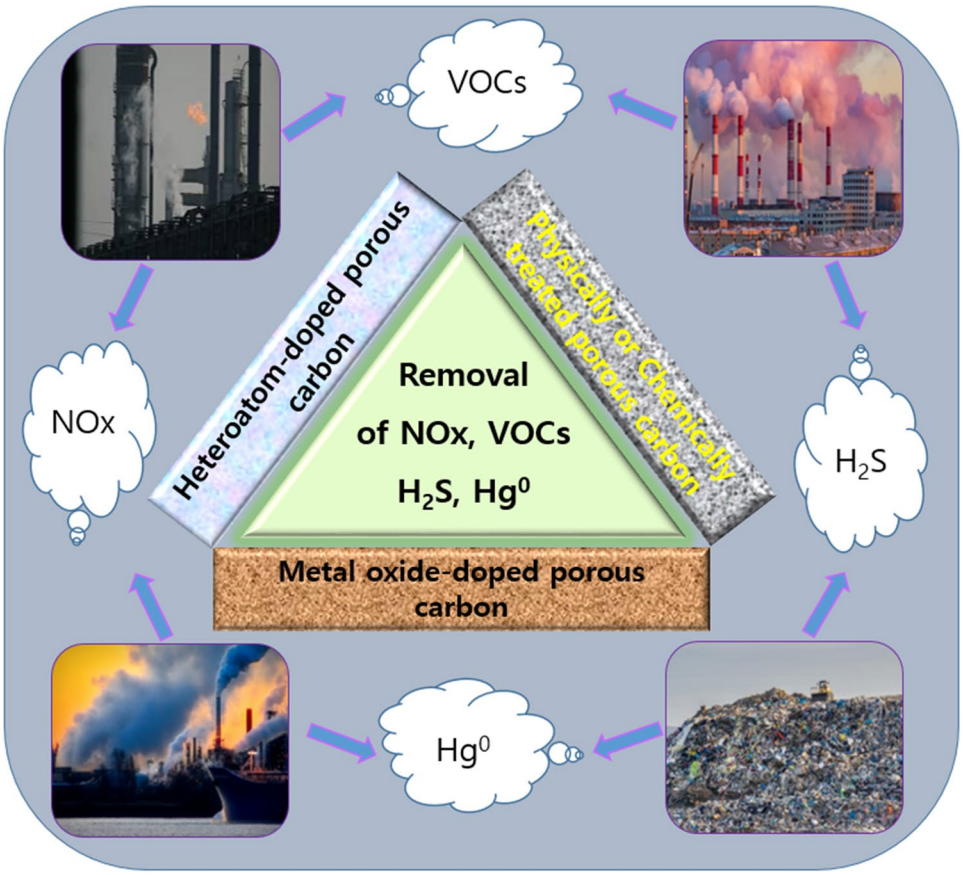


**Fig. 1** Schematic illustration of the removal of toxic gases by modified catalyst with different strategies

physical and/or chemical properties of carbon, which further enhances their air-pollutant-removal efficiency through SCR, catalytic oxidation, or adsorption (Table 2).

### Heteroatom Doping

Heteroatom doping refers to the incorporation of noncarbon elements (such as N, S/P, B, and O) into the carbon lattice. Heteroatom doping introduces new chemical functionalities, such as Lewis acid sites, which can interact with toxic gases and facilitate their adsorption and/or reaction. In addition, the heteroatoms can alter the electronic properties of the carbon lattice and make it more polar and enhance its affinity for polar gas molecules, which further helps control the catalytic reaction or remove toxic gases such as $NO_x$, $H_2S$, $Hg^0$, and toluene (Table 3). Heteroatom doping into porous carbon not only serves as a highly efficient catalyst, but can also be utilized as an ideal support for immobilizing metal nanoparticles (Ma et al. 2016).

Heteroatom doped (S/N) carbon-based single-atom catalyst leads to enhance the high stability, catalytic reaction, and/or electrocatalysis activity (Bai et al. 2023b; Tang et al. 2023b, c); wherein, it observed that benefiting from the synergic action of metal active sites, N-doped graphene nanosheets (FeCo-NG) exhibited higher catalytic performance, i.e. ORR. Anchoring metal on S/N co-doped graphene (Mn-S/N-C) improved the electrocatalytic performance of the catalyst system (Bai et al. 2023b). The d-orbital adjustment of the M-center (Mn) in M-N-S-C catalyst material by S/N co-doping benefits to improve the electrocatalytic activity, which is most superior to previously reported Mn-based electrocatalysts and commercial iridium dioxides. The S-doping and presence of asymmetric structure contributes to the ortho-$Mn_1$-$N_2$-$S_2$G site which is more active than Mn_$N_4$G, Mn-$N_3$SG, para Mn-$N_2$-$S_2$G, and Mn-$NS_3$G sites. The ORR rate-limiting steps on the ortho-$Mn_1$-$N_2$-$S_2C_x$ have been predicted as the transformation of OH* to $H_2O$ (Bai et al. 2023b).

## Applications of Carbon-Based Catalyst for Clean Environmental Remediation

### $NO_x$ Removal

In general, steam/gas purging increases the pore volume (Wang et al. 2016) and develops internal pores by removing trapped volatile gases or particles during carbonization. An increase in the steam-activation temperature enhances the pore volume and specific surface area (SSA) of the

catalyst. The SSAs of PCNF10-800, PCNF10-850, and PCNF10-900—polyacrylonitrile (PAN)-based modified carbon materials—are 778, 876, and 1206 $m^2$/g, respectively, while their total pore volumes are 0.272, 0.315, and 0.562 $cm^3$/g, respectively. Increased surface area and pore volume improve the NO-removal efficiency (Wang et al. 2016). Use of different carbonization and steam-activation temperatures has an obvious impact on the NO conversion. The PCNF catalyst carbonized and steam-activated at 800 °C exhibited 60% NO conversion performance, whereas the catalyst only activated at 800 °C afforded 27.6% NO conversion at room temperature (Table 1). Ku et al. (1994) analyzed the catalytic activity of the coconut-shell-derived activated carbon (AC) prepared via chemical activation using $O_2$-$NH_3$, $H_2SO_4$, and $(NH_4)_2SO_4/H_2SO_4$. The carbon catalyst treated with $(NH_4)_2SO_4/H_2SO_4$ exhibited the highest surface area and catalytic activity (Table 1). Li et al. (2015b) examined the effects of physical activation, chemical activation, and co-activation of the *Sargassum*-based activated carbon (SAC) for low-temperature SCR of $NO_x$. The Co/SAC-2 (co-activated) catalyst afforded the highest NO conversion achieved so far (82.05%) at 125 °C, whereas C/SAC-2 (chemically activated) could afford 75% NO conversion) and P/SAC (physically activated) could afford only 45% NO conversion. Hence, it is clear that chemical co-activation improves the $NO_x$-removal performance.

The porous nature of carbon allows for a better diffusion of gaseous pollutants through the catalyst, which promotes contact between the reactants and the catalyst. Furthermore, carbon modified by metal oxide doping can be utilized for $NO_x$ removal, mostly by low-temperature $NH_3$-SCR. In addition, these superior properties can enhance the tolerance to catalyst poisoning. Zhu et al. reported that doping with 5 wt% of $V_2O_5$ enhanced the $NO_x$-removal efficiency of the AC catalyst from 20 to ~ 80% at 220 °C with a better $SO_2$ poisoning tolerance, which could be owing to the increased catalyst surface acidity because $SO_2$ oxidizes to $SO_4^{-2}$. In addition, the pre-oxidation of the catalyst plays a crucial role in improving the $NO_x$-conversion performance (to up to 98%) (Zhu et al. 1999). Wang et al. (2014) described that doping activated semicoke (ASC) with 3 wt% of $V_2O_5$ improved the SCR catalytic performance (from 25% to > 90%) at 250 °C. Li et al. (2022b) demonstrated that the Ce-modified $V_2O_5$/AC afforded a higher $NO_x$ conversion (i.e., 90%) than that achieved with the unmodified $V_2O_5$/AC (< 80% $NO_x$ conversion) at 200 °C (Table 2). They also discussed the effect of the regeneration temperature (470 °C) and regeneration cycling on the improved SCR performance (i.e., > 95%) of the Ce-$V_2O_5$/AC catalyst. This result suggests that cyclic regeneration is conducive to desulfurization and SCR. Huang et al. (2007) reported that doping CNTs with 2.35 wt% of $V_2O_5$ enhanced the $NO_x$ conversion from < 10 to > 80% at 190 °C. However, $V_2O_5$/CNTs prepared using CNTs with an outer diameter of 60–100 nm afforded better $NO_x$ conversion (92%), perhaps owing to the dispersion of vanadium over the CNT surface and presence of oxygenated groups on the CNT surface with different diameters (during $HNO_3$ treatment). Liu et al. (2021) reported a highly efficient $MnO_x$-doped biochar catalyst obtained by air oxidation for the SCR of $NO_x$, where pre-oxidation (400 °C) and post-oxidation (250 °C) were performed before and after doping $MnO_x$ into the biochar. After pre-oxidation, the SSA and total pore volume of the sample increased from 557 to 734 $m^2$/g and from 0.353 to 0.440 $cm^3$/g, respectively, whereas post-oxidation increased the contents of $Mn^{4+}$ and chemisorbed oxygen, which enhanced the surface acidity and redox capabilities of the catalyst. The catalyst exhibited the highest $NO_x$ conversion, i.e., 97% at 150 °C, compared with that achieved without air oxidation (61.8%). Jiang et al. (2019) investigated the low-temperature $NO_x$-removal performance and high poisoning stability of a MnCe-doped AC and a $V_2O_5$ co-doped MnCe/AC catalyst. The doping of the AC with MnCe enhanced the $NO_x$ conversion from 25 to > 90% at 200 °C. Doping with 0.4 Ce/(Mn + Ce) further increased the $NO_x$ conversion to > 97%. The co-doping of $V_2O_5$ slightly improved the $NO_x$ conversion to > 98%, although it also broadened the reaction window (100–300 °C). In addition, it prevents the active sites from being blocked or poisoned. Figure 2 shows the mechanism of improved $SO_2$ tolerance over the Mn-Ce(0.4)-V/AC catalyst.

Jia et al. (2022) reported $MnO_x$-doped biochar and the effect of the modification method for biochar on the $NO_x$-conversion performance at low temperatures. NaOH-modified biochar doped with 25% $MnO_x$ resulted in the highest $NO_x$ conversion (95%) and a high tolerance to $SO_2$ and $H_2O$ at 225 °C, compared to those achieved with acid- and CTAB-modified biochar. Highly dispersed $MnO_x$ is easily formed on the NaOH-modified biochar surface, which is crucial for improving the SCR performance. Li et al. (2023a) demonstrated that doping coal-based AC with 10 wt% of $Fe_2O_3$ improved the SCR performance from 15 to 30%; however, 10 wt% of $Fe_2O_3$/OAC1.5-60-3 (OAC: oxidized AC with APS oxygen functionalization) dramatically enhanced NO conversion to > 99% at 180 °C. In addition, the reaction temperature window broadened (from 120 to 250 °C) with superior $NO_x$ conversion (> 90%) and high tolerance to $SO_2$ and $H_2O$. This result suggests that the physical structure was not the key factor in the APS oxygen functionalization strategy, which affects the catalyst performance. Xue et al. (2008) reported 100% $NO_x$ conversion of the CuO-impregnated wet oxidized AC (treatment with $H_2O_2$) catalyst at 272 °C, wherein the surface oxygen moieties and NO adsorption on the AC played a crucial role in the production of carbon active sites. Notably, it is not the rate-limiting step for the catalytic reduction of NO over CuO by AC. Zhu et al. (2011) reported that surface-modified AC fibers doped with 9 wt%

**Table 1** Carbon modified through physical/chemical treatment and its performance in removing toxic gases

| Catalyst | Catalyst material source | Physical/chemical treatment conditions | Gas concentration | Surface area ($m^2$/g) | Performance | References |
|---|---|---|---|---|---|---|
| SCA750 | Coal-based AC | Steam activation | 1000 ppm NO, 1500 ppm $NH_3$, 3.5% $O_2$, Ar | 460 | 40% NO conversion, adsorption | Rubel and Stencel (1997) |
| C/SAC-2 | *Sargassum*-based AC | $H_3PO_4$ activation, 500 °C, $N_2$, 1 h | 500 ppm NO, 500 ppm $NH_3$, 5% $O_2$, $N_2$ | 604 | ~75% NO conversion, SCR at 125 °C | Li et al. (2015b) |
| Co/SAC-2 | *Sargassum*-based AC | $H_3PO_4$ activation, 500 °C, $N_2$, 1 h + physical activation at 500 °C with $CO_2$, 1 h | 500 ppm NO, 500 ppm $NH_3$, 5% $O_2$, $N_2$ | | ~82% NO conversion, SCR at 125 °C | Li et al. (2015b) |
| P/SAC | *Sargassum*-based AC | Physical activation at 500 °C with $CO_2$, 1 h | 500 ppm NO, 500 ppm $NH_3$, 5% $O_2$, $N_2$ | | ~45% NO conversion, SCR at 125 °C | Li et al. (2015b) |
| PCNFs | PAN | Carbonization at 800 °C with $N_2$, activated at 800 °C with 30% steam in $N_2$ for 30 min | 20 ppm NO, 21 vol% $O_2$, $N_2$ balanced | 710 | 60% NO conversion, adsorption followed by catalytic oxidation at 30 °C | Wang et al. (2011) |
| PCNF10 | PAN | Carbonization at 800 °C with $N_2$ for 30 min, activated at 850 °C with 20% steam in $N_2$ for 30 min | 20 ppm NO, 21 vol% $O_2$, $N_2$ balanced | 778 | 30% NO conversion, adsorption followed by oxidation at 30 °C | Wang et al. (2016) |
| S9 | Coconut-shell-based AC | $O_2/NH_3$, $H_2SO_4$, $(NH_4)_2SO_4$ treatment at 400 °C | 500 ppm NO, 500 ppm $NH_3$, 3 vol% $O_2$, $N_2$ | 970/1018/1183 | 39/47/67% NO conversion at 150 °C | Ku et al. (1994) |
| AC4 | Cattle manure | Carbonization at 650 °C with $N_2$ for 1 h, activation $CO_2$ flow 1000 mL/min at 850 °C 1 h | 1200 ppm $H_2S$, balance $N_2$, $O_2$ | 408 | 868.45 mg/g, $H_2S$ adsorption capacity at 25 °C, 100 kPas | Tuerhong and Kuerban (2022) |
| CH biochar | Coconut husk | Carbonization at 500 °C for 1 h, activation with $CO_2$/$H_2O$ at 650/750/850 °C | 1 vol% $H_2S$ ($CO_2$ 39%, $CH_4$ 60%) | 332/604/811 | 29.7/38.7/26.7 mg/g $H_2S$-adsorption capacity at 20 °C | Su et al. (2021) |
| PC7PA | Pistachio nutshell | Carbonization at 750/800 °C for 1 h with $H_2O/CO_2$, carbonization at 500/700 °C for 1 h + activation with $CO_2$/$H_2O$ at 900 °C for 1 h | 1 vol% $H_2S$ concentration | 391/877, 277/1204 | 9.4/11.3/7.1/10.5 mg/g $H_2S$-adsorption capacity | Bazan-Wozniak et al. (2017) |
| GS_KOH_1 | Guava seed | Hydrothermal at 200 °C for 48 h, KOH activation for 2 h, carbonization at 900 °C with $N_2$ for 2 h | 20 ppm $H_2S$ | 1682 | 48.18 mmol/g $H_2S$-adsorption capacity at STP | Nicolae et al. (2022) |

**Table 1** (continued)

| Catalyst | Catalyst material source | Physical/chemical treatment conditions | Gas concentration | Surface area ($m^2$/g) | Performance | References |
|---|---|---|---|---|---|---|
| | Oil palm shell | Carbonization at 900 °C for 2 h with $H_2O/CO_2$, KOH/$H_2SO_4$ activation for 24 h + pyrolysis at 700 °C for 2 h | 2000 ppm $H_2S$ balanced with He | 1062/1148/1014 | 46/68/76 mg/g $H_2S$-adsorption capacity at 25 °C | Guo et al. (2007) |
| SAC-800/EAC-800 | Seaweed (*Sargassum/Enteromarpha*) | Pyrolysis at 400–800 °C $N_2$, $ZnCl_2$ activation for 12 h, 400–800 °C, | 80 μg/$m^3$ $Hg^0$, 5 vol% $O_2$, 300 ppm NO, 500 ppm $SO_2$, 3 vol% $H_2O$ | 524/565 | 2382.6/2909.5 μg/g $Hg^0$ removal, adsorption | Liu et al. (2019) |
| C8Br9 | *Sargassum* char | Pyrolysis at 400–800 °C with $N_2$, $NH_4Br$ activation for 12 h at 90 °C | 60 μg/$m^3$ $Hg^0$, 5% $O_2$, 1 vol% $H_2O$, 400 ppm NO, 600 ppm $SO_2$, $N_2$ balanced | 19 | 91% $Hg^0$-removal efficiency, adsorption at 120 °C | Yang et al. (2018) |
| WSW10/RSW10 | Wheat straw/rice stalk | Pyrolysis at 600 °C with $N_2$ for 20 min; activation in a microwave oven with steam at 60 °C for 1 h; chemical treatment with $H_2O_2$ at 30 °C for 1 h | 60 μg/$m^3$ $Hg^0$, 5 vol% $O_2$, 5 vol% $H_2O$, 300 ppm NO, 8000 ppm $SO_2$, $N_2$ | 433/276 | 1293.19/1485.61 μg/g $Hg^0$-adsorption capacity, 130 °C | Li et al. (2021) |
| ACUV9 | AC | $H_2O_2$ steam modification 45 °C with $N_2$; UV irradiation (254 nm, 5 W) at 80 °C for 2 h | 75 μg/$m^3$ $Hg^0$, 400 ppm NO, 600 ppm $SO_2$, $N_2$ | 1373 | 3636.43 μg/g $Hg^0$-adsorption capacity, 120 °C | Dou et al. (2023) |
| MSW3UV | Corn stalk biochar | 600° C carbonization for 20 min; activation with steam + $N_2$ by microwave (700 W) for 30 min; 3% $H_2O_2$ + UV light (254 nm) for 2 h | 65 μg/$m^3$ $Hg^0$, 400 ppm NO, 800 ppm $SO_2$, 5% $O_2$, 65 μg/$m^3$ $Hg^0$, 5% $H_2O$, $N_2$ | 520 | 2052.51 μg/g $Hg^0$-adsorption capacity, 120 °C | Liu et al. (2023b) |
| LPC | Peptone and pork bone | Pyrolysis at 400 °C for 4 h with $N_2$, $K_2CO_3$ treatment, pyrolysis at 800 °C, 1.5 h $N_2$ | 50 μg/$m^3$ $Hg^0$, 400 ppm NO, 500 ppm $SO_2$, 6% $O_2$ | 2926 | 571 mg/g $Hg^0$-adsorption capacity at 150 °C | Wang et al. (2023a) |
| ACAC | Anthracite-coal-based AC | KOH activation, pyrolysis at 700–900 °C for 1 h with $CO_2/N_2$, Br impregnation | 35,000 ng/$m^3$ $Hg^0$, $N_2$ | 527 | 476 μg/g $Hg^0$-adsorption capacity at 100 °C | Song et al. (2020) |
| C6WN5 | Cotton residue | Pyrolysis at 600 °C with $N_2$ for 1 h, Activation for 4 h with microwave + steam, $NH_4Cl$ treatment | 6 vol% $O_2$, 13 vol% $CO_2$, 3 vol% $H_2O$, 300 ppm NO, 1200 ppm $SO_2$, $N_2$ | 203 | 11,400 μg/g $Hg^0$-removal efficiency, adsorption at 120 °C | Li et al. (2015a) |

**Table 1** (continued)

| Catalyst | Catalyst material source | Physical/chemical treatment conditions | Gas concentration | Surface area ($m^2$/g) | Performance | References |
|---|---|---|---|---|---|---|
| TO-Cl | Rice/tobacco/corn/wheat/millet/black bean straw | Carbonization at 600 °C for 1 h, HCl activation for 12 h | 20 μg/$m^3$ $Hg^0$ | 353 | 80 μg/g $Hg^0$-adsorption capacity at 150 °C | Wang et al. (2018a) |
| PHAC/PHAC-AM | Coconut-shell-based carbon | Carbonization at 600–700 °C for 1–4 h, KOH impregnation for 24 h at 105 °C Activation with $CO_2$ and microwave for 4 min, ammonia treatment | 50–250 mg/L toluene | 478/361.8 | 238.10/357.14 mg/g toluene-adsorption capacity at 30 °C | Mohammed et al. (2015) |
| PCS-MClx | Biomass (sodium lignin sulfonate) | Carbonization at 500 °C for 2 h with a metal-chloride-activating agent | 1–10 g/L toluene in paraffin oil | 703 | 2300 mg/g toluene-adsorption capacity at 25 °C | Li et al. (2020a) |
| SRC-3K700/800 | Waste soybean residue | Pre-carbonization at 450 °C, KOH activation at 500–800 °C | 250 ppm toluene | 4293/3603 | 1587/2187 mg/g toluene-adsorption capacity at 25 °C | Li et al. 2022a) |
| NHPC-CC | Corn straw, wheat stalk, bamboo, pine, corncob | $(NH_4)_2C_2O_4{\cdot}H_2O$ and $KHCO_3$ + carbonation at 900 °C with $N_2$ for 1 h | 300 ppm toluene | 2266 | 5.94 mmol/g toluene-adsorption at 30 °C | Huang et al. (2023) |

**Table 2** Metal oxide-doped carbon and its toxic gas-removal performance

| Catalyst | Support material condition | Metal oxide-doping conditions | Gas concentration | Surface area ($m^2/g$) | Performance | References |
|---|---|---|---|---|---|---|
| 5 wt% $V_2O_5$/AC | Coal-derived semicoke + $HNO_3$ activation | Pore volume impregnation, calcination at 300–600 °C; peroxidation at 250 °C for 5 h | 500 ppm NO, 560 ppm $NH_3$, 3.3% $O_2$, Ar balanced | | 98% $NO_x$ conversion at 220 °C (SCR) | Zhu et al. (1999) |
| 3 wt% $V_2O_5$/ASC | Activated semicoke + $HNO_3$ activation + calcination at 700 °C for 4 h with Ar | Impregnation + calcination at 500 °C for 5 h with Ar, pre-oxidation in air at 200 °C for 2 h | 1000 ppm NO, 1000 ppm $NH_3$, 2% $O_2$, Ar balanced | 220 | > 90% $NO_x$ conversion at 250 °C (SCR) | Wang et al. (2014) |
| Ce-V/AC | AC HCl + HF treatment | V-Impregnation + calcination at 500 °C with $N_2$ for 8 h, air oxidation at 250 °C for 5 h; Ce-impregnation at 400 °C in $N_2$ for 2 h | 500 ppm NO, 500 ppm $NH_3$, 5 vol% $O_2$, $N_2$ balanced | 966 | 90% $NO_x$ conversion at 200 °C (SCR) | Li et al. (2022b) |
| 2.35 wt% $V_2O_5$/CNT | Multiwall CNT prepared by CVD + $HNO_3$ treatment | Incipient impregnation, calcination at 350 °C for 2 h | 800 ppm NO, 800 ppm $NH_3$, 5 vol% $O_2$, He balanced | 368.254 | 92% $NO_x$ conversion at 463 K | Huang et al. (2007) |
| MnCe(0.4)V/AC | AC + $HNO_3$ treatment | Ultrasonic impregnation, calcination in Ar at 400 °C for 4 h | 500 ppm NO, 500 ppm $NH_3$, 5 vol% $O_2$, $N_2$ balanced | 723 | 98% $NO_x$ conversion at 200 °C (SCR) | Jiang et al. (2019) |
| BC-OMO | Coconut shell biochar, calcination at 400 °C under $O_2$/$N_2$ for 2 h, post-oxidation at 250 °C | Impregnation, calcination at 250 °C for 2 h in air | 400 ppm NO, 440 ppm $NH_3$, 5 vol% $O_2$, $N_2$ balanced | 734 | 97% $NO_x$ conversion at 150 °C (SCR) | Liu et al. (2021) |
| 25% Mn/LBC-OH | Lotus leaf + NaOH treatment and calcined at 800 C with $N_2$ for 2 h (LBC-OH) | Ultrasonic impregnation, calcination at 400 °C for 2 h with $N_2$ | 600 ppm NO, 600 ppm $NH_3$, 50 ppm $SO_2$, 2.5 vol% $O_2$, $N_2$ balanced | 377.5 | > 95% $NO_x$ conversion at 225 °C | Jia et al. (2022) |
| 10 wt% $Fe_2O_3$/OAC1.5–60-3 | Coal-based AC + $(NH_4)_2S_2O_8$ oxidation | Ultrasound impregnation, calcination at 400 °C for 4 h, $N_2$ | 550 ppm NO, 550 ppm $NH_3$, 5 vol% $O_2$, 200 ppm $SO_2$, $N_2$ balanced | | > 99% $NO_x$ conversion, SCR at 180 °C | Li et al. (2023a) |
| 15 wt% CuO/AC-H | Coconut-shell-based AC + $HNO_3$/$H_2O_2$/$H_2SO_4$ activation | Wet impregnation, calcination at 250 °C for 4 h | 2000 ppm NO, Ar balanced | 1038/1064/796 | ~ 100% $NO_x$ conversion, SCR at 272 °C | Xue et al. (2008) |
| 9 wt% $CeO_2$ ACFN/AACFP | Viscose-based AC + $HNO_3$/low-temperature oxygen plasma treatment | Impregnation, calcination at 350 °C for 6 h with $N_2$ | 1000 ppm NO, 1000 ppm $NH_3$, 5% $O_2$, Ar | 874/1124 | 93.96/86% NO conversion, SCR at 180 °C | Zhu et al. (2011) |
| $ZnO_{0.2}$-$MgO_{0.8}$/AC | Coal-based AC | Impregnation at 350 °C for 2 h with $N_2$ | 850 mg/$m^3$ $H_2S$, balance $N_2$, $O_2$ | 653 | 113.4 mg/g, $H_2S$ adsorption capacity at 30 °C, 100 kPas | Yang et al. (2020b) |

**Table 2** (continued)

| Catalyst | Support material condition | Metal oxide-doping conditions | Gas concentration | Surface area ($m^2$/g) | Performance | References |
|---|---|---|---|---|---|---|
| $ZnO_{(0.5)}$-$CuO_{(0.5)}$/AC | Lignite-based AC | Incipient wetness impregnation, thermal treatment at 250 °C with $N_2$ for 3 h | 3000 ppmv $H_2S$ (in $N_2$) | 570 | 50 mg/g $H_2S$ adsorption capacity at 30 °C, 100 kPas | Balsamo et al. (2016) |
| ZnO-CuO/AC | AC | Incipient wetness impregnation, thermal treatment at 250 °C with $N_2$ for 3 h | 3000 ppmv $H_2S$ | 570 | 1.46 mmol/g $H_2S$-adsorption capacity at 30 °C | de Falco et al. (2018) |
| ZFOB-10 | BAX-wood-based carbon phosphoric acid activation | Wet impregnation, calcination at 400 °C for 4 h | 1000 ppm $H_2S$ | 1403 | 122.5 mg/g $H_2S$-adsorption capacity | Yang et al. (2020a) |
| 1 wt% Mn/AC | AC | Pore volume impregnation, calcination at 400 °C for 4 h with $N_2$ | 3000 ppm $H_2S$ | 905 | 142 mg/g, $H_2S$-catalytic oxidation at 180 °C | Fang et al. (2013) |
| Cu2.56WRS300 | Rice straw (RS)-based biochar + microwave steam activation 30 min | RS pyrolysis at 600 °C for 20 min with $N_2$, impregnation, calcination at 200/300/400 °C for 1.5 h with $N_2$ | 250 ppm $H_2S$ (in $N_2$) | 51/60/32 | 1191.1 mg/g $H_2S$-adsorption capacity at 125 °C | Cui et al. (2022) |
| MCS-MgO-15 | Resorcinol, formaldehyde | Carbonization at 800 °C for 3 h, MgO treatment 400 °C with $N_2$ for 3 h | 1000 ppm $H_2S$, 1% $O_2$, $N_2$ balanced | 660 | 2.46 g/g, $H_2S$-catalytic oxidation at 30 °C | Zhang et al. (2016) |
| 6% $Co_{0.5}Cr_{0.5}$/AC | Activated coke + pretreatment with $HNO_3$ | Ultrasound impregnation, pyrolysis 500 °C with $N_2$ for 6 h | 100 μg/$m^3$ $Hg^0$, 6 vol% $O_2$, $N_2$ balanced | 217.72 | 88.3% $Hg^0$-removal, adsorption, and catalytic oxidation at 240 °C | Gao et al. (2023) |
| 15% $Co_{0.4}Ce_{0.6}$/BAC | Maize straw, $ZnCl_2$ impregnation, activation at 750 °C for 2 h with $N_2$, $HNO_3$ treatment (BAC) | Impregnation, calcination at 550 °C with $N_2$ for 4.5 h | 100 μg/$m^3$ $Hg^0$, $N_2$ balanced | 628.85 | 96.8 μg/g $Hg^0$-adsorption capacity, 230 °C | Gao et al. (2018) |
| 15% $Co_{0.4}Mn_{0.6}$/BAC | Maize straw, $ZnCl_2$ impregnation, activation at 750 °C for 2 h with $N_2$, $HNO_3$ treatment (BAC) | Ultrasound impregnation, calcination at 500 °C with $N_2$ for 4 h | 100 μg/$m^3$ $Hg^0$, $N_2$ balanced | 617.14 | 98.5% $Hg^0$-removal efficiency, adsorption at 240 °C | Gao et al. (2019) |
| $CuFe_{0.3}$/WSWU10(500) | Wheat straw, pyrolysis at 600 °C for 20 min under $N_2$ (WS), microwave + steam activation | Ultrasound impregnation, calcination at 500 °C with $N_2$ for 1 h | 65 μg/$m^3$ $Hg^0$, $N_2$ | 253.49 | 2276.45 μg/g $Hg^0$-adsorption capacity, 130 °C | Yang et al. (2019) |
| MnFe/Char-BM4 | Rice straw | Ball milling for 4 h at 25 Hz, followed by 800° C pyrolysis for 1 h | 35 μg/$m^3$ $Hg^0$, 5% $O_2$, $N_2$ | 311.4 | > 95% $Hg^0$-removal efficiency, adsorption at 100 °C | Zhang et al. (2021) |
| AC03 (3 wt% CuO/AC) | Commercial AC | Ultrasonication for 15 min, kept for 12 h at RT, calcination at 250 °C for 2 h | 33,803 mg/$m^3$ toluene | 985.2 | 701.8 mg/g toluene-adsorption capacity at 20 °C | Lei et al. (2020) |

**Table 2** (continued)

| Catalyst | Support material condition | Metal oxide-doping conditions | Gas concentration | Surface area ($m^2/g$) | Performance | References |
|---|---|---|---|---|---|---|
| $CuCo_{0.5}/C$ | 1,3,5-Benzene tri-carboxylic acid | Solvothermal method (Cu-BTC) + calcination at 500 °C for 2 h in Ar and air at 500 °C for 2 h each. Co impregnation + calcination at 500 °C in Ar and air for 2 h each | 1000 ppm toluene | 22.9 | 90% toluene oxidation at 243 °C | Li et al. (2020b) |

of $CeO_2$ exhibited high $NO_x$ conversion (93.96%) at 180 °C; the surface modification of the ACF by $HNO_3$ afforded a better catalytic activity (i.e. > 90%) over a broad temperature window (150–240 °C) compared to that achieved with the oxygen plasma treatment (< 85% $NO_x$ conversion).

Heteroatom doping (especially that of N) into carbon can be used to modify its physical and chemical properties to enhance the $NO_x$-removal performance (Table 3). Li et al. (2014) reported the effects of impregnation duration (5 h) and calcination temperature (900 °C) on the N-content and $NH_3$-SCR activity of the modified AC. ACM-5–900 exhibited 51.67% of NO conversion at 80 °C, while that shown by undoped AC was 21.92%. However, they demonstrated that the form of N-containing functional groups {ACM-5–900 had highest proportion of N-6 (pyridinic-N) groups, i.e., 57.3%} influenced NO conversion rather than the total N-content. In addition to the impregnation duration, the N-doped precursor also played a crucial role in improving the $NO_x$ conversion of the modified AC, as shown schematically in Fig. 3. The N-doped ACM-5 catalyst with a $KHCO_3$ promoter exhibited a higher $NO_x$-conversion efficiency (52%) than that the reported N-doped carbon catalysts (30%). In contrast, undoped AC showed only 10% $NO_x$-conversion efficiency (Li et al. 2020d). N-6 was reported as an activated site for the catalytic direct decomposition of NO at 500 °C in N-doped porous carbon; in the absence of N-doping, the carbon catalyst showed only < 10% NO conversion (Wang et al. 2018b). Yao et al. (2020) reported the N-doped semicoke-based catalyst, i.e., ASC-10U10Mn, with a high $NO_x$ conversion of 94.5% at 275 °C, while the ASC showed 10% $NO_x$ conversion. They also demonstrated that N-groups with unpaired electrons (N-6, N-5 pyrrolic, and N-Q- quaternary) play a crucial role in enhancing the adsorption and oxidation of NO and $NH_3$ adsorption owing to abundant Lewis acid sites. N-doping also improves the electron distribution of the catalyst and the electron mobility between the Mn and oxygen moieties. Figure 4 shows the promotion mechanism of N-doping over the $MnO_x$/semicoke catalyst for low-temperature SCR.

Lin et al. (2018) reported the effects of N-dopant precursors/additives on the SCR of $NO_x$ over the modified AC, where the N-doped AC with the pyridine additive/precursor exhibited a higher $NO_x$ conversion (66%) than that achieved with other catalysts. Zhu et al. (2019) investigated the influencing mechanism of N-doping on $NO_2$ adsorption and reduction over the AC using computational studies. AC600 with a higher N-content exhibited the highest $NO_2$-adsorption capacity (135.6 mg/g) and the lowest NO-release percentage. Li et al. (2020c) reported N-doped porous biochar with 82% $NO_x$ conversion at 260 °C, where N-6 played a major role in boosting up the denitrification activity. However, raw biomass reacts more readily with N-containing additives, which facilitates carbon formation

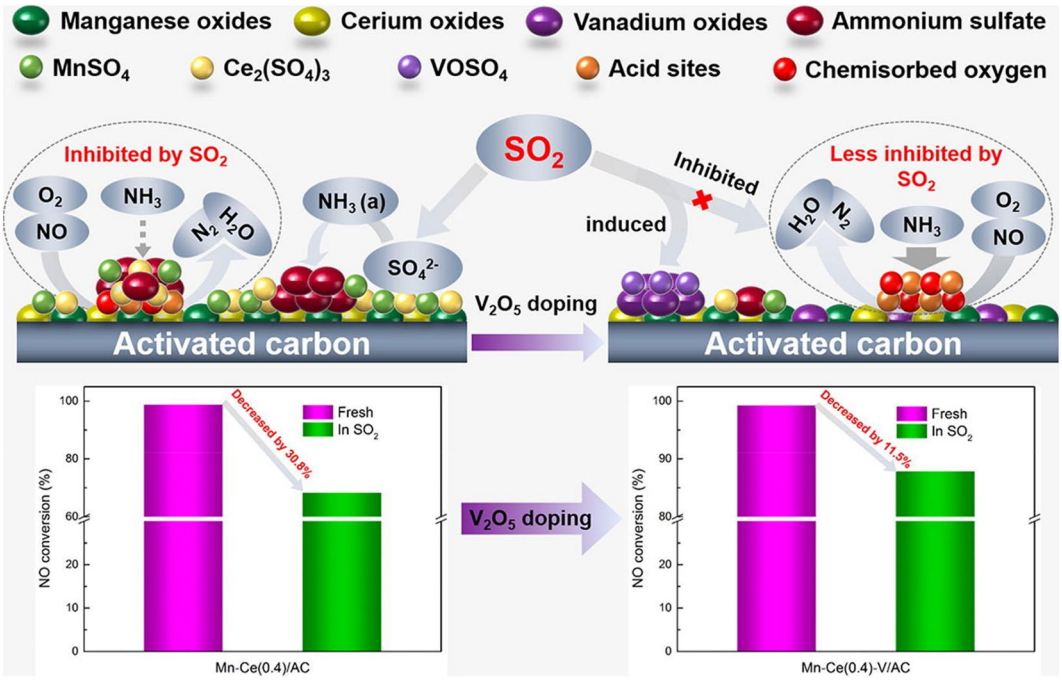


**Fig. 2** Mechanism of better $SO_2$ tolerance over Mn-Ce(0.4)-V/AC and effect of V-oxide doping over SCR of NO (Jiang et al. 2019)

with an ultrahigh N-content, resulting in the formation of modified carbon with an N-content of 17.71 at. % (N-6: 9.09 at.%). This modified carbon catalyst demonstrated > 90% of NO conversion at 200 °C, which is higher than that achieved with non-N-doped carbon (< 20%). Li et al. (2023b) investigated the synergistic effect of dual heteroatom dopants (N and O) on the carbon-catalyzed $NH_3$ SCR of $NO_x$. The N- and O-doped AC (NOAC) was prepared through one-step $NH_3{\cdot}H_2O$ activation of the AC, followed by $HNO_3$ oxidation. The NOAC exhibited enhanced $NO_x$ conversion at 200 °C (~ 90%) compared to that shown by the O-doped (~ 62%) or N-doped AC (~ 73%); non-doped AC exhibited only 30% of $NO_x$ conversion. In addition to N and O dopants, B and P dopants in carbon catalysts also demonstrated effective $NH_3$ SCR of $NO_x$ (Li et al. 2020e; Yang et al. 2021), wherein the Lewis acid properties of the dopants can enhance the adsorption and activation of the reactants ($NH_3$ and $O_2$).

## $H_2S$ Removal

Physically and chemically activated carbon can also be utilized for $H_2S$ removal, mainly by physi-/chemisorption. Physisorption is a relatively weak, nonspecific adsorption that involves intermolecular forces between the adsorbate ($H_2S$) and the adsorbent (with carbon as the solid surface). Physisorption of $H_2S$ occurs when weak van der Waals forces form between the sulfur atoms of $H_2S$ and the surface atoms or molecules of the adsorbent material. Physisorption is reversible and typically occurs at low temperatures and high pressures. It does not involve any significant chemical changes to the adsorbate or adsorbent. In contrast, chemisorption is a stronger, specific adsorption that involves the formation of chemical bonds between the adsorbate and the adsorbent. Chemisorption of $H_2S$ occurs when its sulfur atom forms chemical bonds with the atoms or molecules on the adsorbent surface. Chemisorption typically involves breaking and forming of chemical bonds, leading to a more stable adsorption state. Chemisorption is generally irreversible and can occur at lower pressures and higher temperatures than physisorption. Cattle manure-based AC catalysts are generally prepared through steam and $CO_2$ activation at 850 °C to remove $H_2S$. The AC4 catalyst prepared by pyrolysis at 650 °C and activated with $CO_2$ exhibited the highest SSA (408.36 $m^2/g$) and $H_2S$ adsorption capacity (868.45 mg/g) compared to those of AC (AC3) activated with steam. These results indicated that pH and surface area, rather than porosity, are crucial factors for the $H_2S$ adsorption (Tuerhong and Kuerban 2022). Su et al. also reported an enhanced surface area with an increase in the pyrolysis temperature, wherein the coconut husk carbonized at 500 °C showed small SSA (0.18 $m^2/g$), which dramatically increased after activation at 650 °C (331.9 $m^2/g$), 750 °C (604.1 $m^2/g$), and 850 °C (811.4 $m^2/g$). However, the surface area does not follow the same trend as that followed by the $H_2S$-adsorption capacity; the adsorption capacities of the catalyst activated at 650, 750, and 850 °C are 29.7, 38.7, and 26.7 mg/g, respectively (Table 1). Therefore, the $H_2S$-adsorption capacity is not entirely dependent on

**Table 3** Heteroatom-doped carbon and its toxic gas-removal performance

| Catalyst | Dopant source | Carbon source + activator/porogen | Doping experimental conditions | Gas concentration/pressure used | Surface area ($m^2/g$) | Performance | References |
|---|---|---|---|---|---|---|---|
| ACM-5–900 | Melamine (N) | Coal-based AC | Impregnation at RT for 1/3/5/7 h, carbonization at 600/700/950 °C for 40 min | 0.05% NO, 0.05% $NH_3$, 5% $O_2$, 0.01% $SO_2$, $N_2$ balanced | 816 | 51.67% NO conversion at 80 °C (SCR) | Li et al. (2014) |
| ACM-5 | Melamine (N) | Coal-based AC + $KHCO_3$ | Impregnation for 1/3/5/7 h, calcination at 900 °C for 40 min in $N_2$ | 500 ppm NO, 500 ppm $NH_3$, 5 vol% $O_2$, $N_2$ balanced | 830 | 52% $NO_x$ conversion at 150 °C (SCR) | Li et al. (2020b) |
| NPC-500 | Melamine (N) | EDTA + KOH | Thermal condensation, carbonization at 450/500/550 °C 0.5 h with Ar | 400 ppm NO, Ar balanced | 341 | > 93% NO decomposition at 500 °C | Wang et al. (2018b) |
| ASC-10U10Mn | Urea (N) | ASC (activated semicoke) | Wet impregnation, calcination at 400 °C for 6 h with $N_2$ | 0.05% NO, 0.05% $NH_3$, 5% $O_2$, 0.01% $SO_2$, 5% $H_2O$, $N_2$ balanced | 38 | 94.5% $NO_x$ conversion, SCR at 275 °C | Yao et al. (2020) |
| AC-4 | Pyridine/Pyrrole/Melamine/Urea (N) | Anthracite AC | Heating at 900 °C with $N_2$ for 2 h, carbonation at 600 °C with $N_2$ for 1 h | 500 ppm NO, 500 ppm $NH_3$, 5 vol% $O_2$, $N_2$ balanced | 111 | 66% $NO_x$ conversion at 150 °C (SCR) | Lin et al. (2018) |
| RH/K/M | Melamine (N) | Rice Husk + KOH | Carbonization at 800 °C under $N_2$ for 2 h | 400 ppm NO, 400 ppm $NH_3$, 5 vol% $O_2$, $N_2$ balanced, $H_2O$ 2.5%, $SO_2$ 100 ppm | 452 | 90% $NO_x$ conversion at 200 °C (SCR) | Li et al. (2020a) |
| NMAC-1.5–7 | Urea (N) | Cotton stalk based biochar + $H_3PO_4$ | $H_3PO_4$ impregnation at 1.5 h, carbonization at 600 °C with $N_2$ for 2 h, biochar + urea 24-h mixing calcined at 500 °C for 1 h with $N_2$ | 500 ppm NO, 500 ppm $NH_3$, 5 vol% $O_2$, $N_2$ balanced | 954 | 82% $NO_x$ conversion at 260 °C | Liu et al. (2023a) |
| P-CA-$800_{vac}$ | Phosphoric acid (P) | m-cresol, Phenol | One pot sol–gel, carbonization at 600–900 °C for 3 h with $N_2$, heat treatment at 380 °C under vacuum for 8 h | 500 ppm NO, 500 ppm $NH_3$, 5 vol% $O_2$, $N_2$ balanced | 315 | 76.8% NO conversion at 200 °C SCR | Li et al. (2020e) |
| B-CA | Phenyl boronic acid | Catechol, Resorcinol | Sol–gel, heat treatment at 400 °C for 1 h with $N_2$ | 500 ppm NO, 500 ppm $NH_3$, 5 vol% $O_2$, $N_2$ balanced | 512 | 96% $NO_x$ conversion at 120 °C (SCR) | Yang et al. (2021) |
| NOAC | $NH_3{\cdot}H_2O$ (N) | Coal-based AC + $HNO_3$ oxidation | $NH_3{\cdot}H_2O$ activation at 900 °C for 1 h in $N_2$ atmosphere | 500 ppm NO, 500 ppm $NH_3$, 5 vol% $O_2$, 200 ppm $SO_2$, 5/10% $H_2O$, $N_2$ balanced | 1350 | ~90% $NO_x$ conversion at 200 °C (SCR) | Li et al. (2023b) |

**Table 3** (continued)

| Catalyst | Dopant source | Carbon source + activator/porogen | Doping experimental conditions | Gas concentration/pressure used | Surface area ($m^2/g$) | Performance | References |
|---|---|---|---|---|---|---|---|
| A-N-OMC-700 | m-aminophenol (N) | Block copolymer F127 | Carbonization at 700–900 °C for 1 h with $N_2$, KOH activation at 800 °C for 2 h | 500 ppm $H_2S$, 2500 ppm $O_2$, balanced $N_2$ | 1538 | 10.5 mmol/g $H_2S$-adsorption capacity at 0 °C, 1 bar | Liang et al. (2020) |
| N-OMCS-700 | m-aminophenol with HMTA (N) | Block copolymer template F127 | Hydrothermal curing at 95 °C for 12 h, carbonization at 700–900 °C, air oxidation at 250 °C 2 h, KOH activation at 800 °C for 2 h under $N_2$ | 5000 ppm $H_2S$, 2500 ppm $O_2$, balance $N_2$, | 1575 | 13.4 mmol/g, $H_2S$-adsorption capacity at 0 °C, 1 bar | Kan et al. (2019) |
| YC-0.5–2(7) | Melamine cyanurate (N) | Poplar saw dust | KOH treatment 5 min, drying at 105 °C for 24 h, carbonization at 800 °C for 2 h with $N_2$ | 0.05 vol% $H_2S$, 0.5 vol% $O_2$, balanced $N_2$ | 678 | 1872 mg/g $H_2S$-adsorption capacity at 25 °C | Wu et al. (2022) |
| NPC-1 | Carbon nitride (N) | Cypress saw dust | Magnetic stirring 3 h, pyrolysis at 800 °C with $N_2$ for 2 h | 1000 ppm $H_2S$ (in $N_2$) | 1839 | 426 mg/g $H_2S$-adsorption capacity at 30 °C, 100 kPas | Chen et al. (2021) |
| KHC-1 | Waste Polyurethane foam | Waste Polyurethane foam powder | Hydrothermal carbonization at 160–220 °C for 2–15 h, $K_2CO_3$ activation at 800 °C for 1 h with $N_2$ | 1000 ppmv $H_2S$ | 1419 | 205.06 mg/g $H_2S$-adsorption capacity at 25 °C | Chen et al. (2020) |
| HNBC | Urea (N) | Cypress saw dust + $H_2O_2$ treatment | Hydrothermal treatment at 190 °C for 12 h, Calcination at 900 °C 4 h | 500 ppm $H_2S$, 10,000 ppm $O_2$, balance $N_2$, | 841 | 181 mg/g $H_2S$-adsorption capacity at 25 °C | Chen et al. (2022) |
| NC-700–2 | Urea phosphate (N) | Sawdust | Impregnation, calcination at 700–900 °C for 2 h with $N_2$ | 100 ppmv $H_2S$ | 1189 | 54.80 mg/g $H_2S$-adsorption capacity at 30 °C | Ma et al. (2021) |
| HNMC-800 | Ethylene diamine | Pyromellitic dianhydride | Hydrothermal treatment 180 °C for 12 h, pyrolysis at 700–1000 °C for 2 h with $N_2$ | 0.5 vol% $H_2S$, 0.25 vol% $O_2$, balanced $N_2$ | 330.5 | 100% $H_2S$ conversion at 150 °C | Lei et al. (2023) |
| JW-NC-4–900-120 | Jute waste biomass (N and S) | Jute waste biomass | Carbonization at 600 °C for 1 h with $N_2$, magnetic stirring, KOH activation at 700–900 °C | | 2579 | 17.19 mmol/g $H_2S$-adsorption capacity at 1 bar | Ahmadi et al. (2021) |
| $PBC_{900}$ | $H_3PO_4$ (P) | Waste wood | Agitation for 2 h, pyrolysis at 700–900 °C with $N_2$ for 1 h | 90 μg/$m^3$ $Hg^0$, 3–9 vol% $O_2$, $N_2$ balanced | 1038 | 15,047.64 μg/g $Hg^0$-adsorption capacity, 100 °C | Zhou et al. (2022a) |

**Table 3** (continued)

| Catalyst | Dopant source | Carbon source + activator/porogen | Doping experimental conditions | Gas concentration/pressure used | Surface area ($m^2/g$) | Performance | References |
|---|---|---|---|---|---|---|---|
| SMC-900 | 2-Thiophene (S) | Thymol blue | Template method, impregnation, carbonization for 2 h at 700–900 °C with $N_2$ | 27 μg/$m^3$ $Hg^0$, 6% $O_2$, $SO_2$ 0–1260 ppm, $N_2$ balanced | 933 | > 97% $Hg^0$ removal at 50–150 °C | Zhou et al. (2022b) |
| NSDG-10 | Cabbage + Thiourea (N,S) | Cabbage waste | Pyrolysis at 400 °C with $N_2$, KOH activation at 850 °C with $N_2$ | | 504 | 2100 μg $Hg^0$-adsorption capacity, 100 °C | Vakili et al. (2021) |
| NPC-1 | Urea (N) | Kelp Biomass | Carbonization at 500 °C for 2 h, KOH treatment for 6-h mixing and heating at 800 °C for 1 h with $N_2$ | 50–1000 ppm toluene | 3235 | 691.1 mg/g toluene-adsorption capacity at 30 °C | Jin et al. (2022a)) |
| PSAC-K-N | Melamine (N) | Pistachio shell + $NaHCO_3$ and $K_2CO_3$ activator | Impregnation with an activator, carbonization activation at 700 °C for 2 h with $N_2$ | 110 mg/$m^3$ toluene | 1000 | 223 mg/g toluene-adsorption capacity at 30 °C | Cheng et al. (2023) |
| NOHC-gr | Urea (N, O) | Biomass | Carbonization at 900 °C for 2 h with $N_2$ | 2.5 kPa | 1650 | 627 mg/g toluene-adsorption capacity at 15 °C | Du et al. (2020) |
| NC900 | Ammonia gas (N) | Cork biomass carbon | Pre-carbonization in $N_2$ at 800 °C for 1 h, activation with $NH_3$ at 700–900 °C for 1 h | 3 kPa | 2060 | 720 mg/g toluene-adsorption capacity at 25 °C | Xu et al. (2021) |
| NHPC-CC | $(NH_4)_2$ $C_2O_4$ (N) | Biomass + $KHCO_3$ | Carbonization activation at 900 °C for 1 h with $N_2$ | 500 ppm toluene | 2266 | 5.94 mmol/g toluene-adsorption capacity at 30 °C | Huang et al. (2023) |
| $MUF_2$-800 | Melamine Urea (N) | Urea, Formaldehyde | Carbonization at 400 °C for 1 h with $N_2$, KOH activation at 500–800 °C for 1 h with $N_2$ | 3.8 kPa | 2578 | 813.6 mg/g toluene-adsorption capacity at 25 °C | Shi et al. (2022a) |

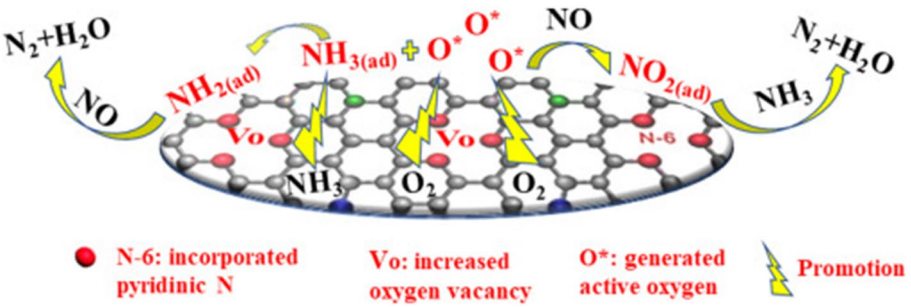


**Fig. 3** Promotional effect of N-doping that improves the $NO_x$ conversion of modified AC (Li et al. 2020b)

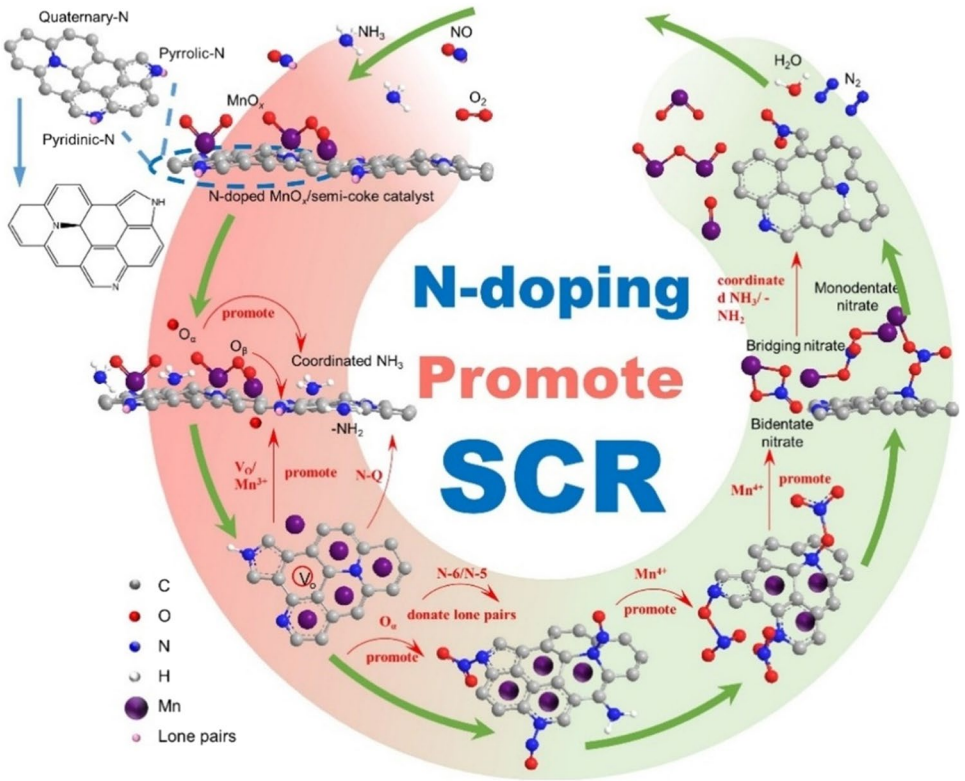


**Fig. 4** Promotional mechanism of N-doping on $MnO_x$/semicoke catalyst for low-temperature SCR (Yao et al. 2020)

the SSA; instead, it is related to the pore size distribution (Su et al. 2021). Similarly, Bazan et al. suggested that the SSA and micropore volume are crucial for enhancing the $H_2S$-adsorption capacity of pistachio nutshell-based catalysts prepared via $H_2O/CO_2$ activation. When the total and micropore volumes of the pistachio nutshell-based catalyst were 0.19 and 0.14 $cm^3/g$, respectively, the $H_2S$ adsorption was 7.1 mg/g, which further increased to 11.3 mg/g with an increase in the total and micropore volume (0.64/0.54 $cm^3/g$) of the catalyst. The SSA is another important factor that affects adsorption under wet conditions (Bazan-Wozniak et al. 2017). Nicolae et al. (2022) reported that the pore volume, rather than the SSA, affects the $H_2S$-adsorption performance. KOH activation of the GS_KOH_1 catalyst prepared using guava seeds by hydrothermal carbonization has more micropores, which increase the gas uptake (48.18 mmol/g; in contrast, the GS_KOH_1 catalyst without KOH activation demonstrated an uptake of only 1.52 mmol $g^{-1}$), compared to the carbon catalyst activated with $H_3PO_4$ and $K_2CO_3$ that exhibited micropore volumes of 0.46 and 0.58 $cm^3/g$ with $H_2S$-adsorption capacities of 7.1 and 11.3 mg/g, respectively (Bazan-Wozniak et al. 2017). Guo et al. also reported that the chemical activation and micropore volume of oil palm fiber-based AC enhanced the $H_2S$-removal performance (68/76 mg/g; KOH/$H_2SO_4$ activation) compared to that achieved by physical activation (48 mg/g, $CO_2$ activation) (Table 1). $H_2SO_4$-activated carbon has a larger micropore volume (0.28 $cm^3/g$) than that of KOH-activated carbon (0.25 $cm^3/g$) (Guo et al. 2007). Hence, it is clear that $H_2S$ removal is affected by the combined effects of the SSA, pore volume (total/micro), humidity, and functional moieties.

Doping porous carbon catalysts with metal oxides can modify the physical and chemical properties of such catalysts, which would in turn improve the adsorption capacity

of these catalysts for $H_2S$. AC was doped with various metal oxides (such as ZnO, MgO, CuO, $ZnFe_2O_4$, $MnO_x$, $V_2O_5$, $CoO_x$, and $CeO_2$) to improve the adsorption and catalytic oxidation of $H_2S$ (Table 2). Yang et al. (2020b) reported that $MgO_{0.2}ZnO_{0.8}$-doped AC exhibited the highest $H_2S$-adsorption capacity (113.4 mg/g among catalysts with different molar ratios of Mg/(Mg + Zn) at 30 °C). The $H_2S$-removal performance was linked to MgO; its basicity continuously increased the formation of $HS^-$ for reactive adsorption on active ZnO and for its catalytic oxidation to elemental sulfur. Doping of AC with Zn and Cu oxides (i.e., $Cu_{0.5}Zn_{0.5}O$/AC) afforded 50 mg/g of $H_2S$-adsorption capacity at 30 °C, which is higher than that achieved with ZnO/AC (33 mg/g). Doping with low amounts of Cu reduced the diffusional limitations in the lattice of the active of the composite phase and through the reacted overlayer—a known issue for ZnO-based sorbents at low temperatures (Balsamo et al. 2016; de Falco et al. 2018). Yang et al. (2020a) reported the use of 10 wt% $ZnFe_2O_4$-doped AC as a reusable adsorbent for $H_2S$ removal. It is regenerated at 500 °C and exhibits a higher adsorption capacity (122.5 mg/g) at room temperature than that achieved with AC (5.6 mg/g) and $ZnFe_2O_4$ (1.6 mg/g) alone. This result reveals the synergistic effect between $ZnFe_2O_4$ and AC on the removal of $H_2S$. AC was doped with various metal oxides (such as Mn, Cu, Fe, Ce, Co, and V) to observe the effects of metal oxide doping on their $H_2S$-adsorption capacities. The Mn oxide-doped AC catalyst exhibited the highest $H_2S$-adsorption capacity (142 mg/g) among all the catalysts. This high capacity remained unaffected even after four consecutive adsorption–regeneration cycles. The SSA of all the metal oxide-doped AC catalysts increased only slightly from 876 to 905 $m^2/g$, which is an unusual behavior (Fang et al. 2013). The copper-oxide-doped biochar exhibited an outstanding $H_2S$-adsorption capacity (1191.1 mg/g) at 125 °C, wherein along with the metal oxide concentration, the microwave steam activation and calcination temperature also played a crucial role in enhancing the $H_2S$-adsorption efficiency (Cui et al. 2022). Zhang et al. (2016) reported an MCM-MgO-15 catalyst with the highest $H_2S$-adsorption capacity (2.46 g/g) along with a high total pore volume (1.74 $cm^3/g$) (Table 2). They prepared AC from resorcinol with carbonation at 800 °C, followed by the caustic impregnation of MgO. The caustic impregnation and its loading determine the performance of the catalyst; however, MgO performed better than conventional salts did, such as $Na_2CO_3$, NaOH, $K_2CO_3$, and KOH. Hence, the surface area was not a major factor affecting the $H_2S$-removal performance; instead, large pores and high mesoporosity are essential for improved $H_2S$ removal.

Heteroatom doping is considered an efficient strategy for promoting the catalytic process of carbon, such as desulfurization (Table 3). In particular, N-doped carbon can act as a basic site, enhancing the electron-donating ability of the carbon lattice, and further increasing its redox activity and corrosion resistance. Liang et al. (2020) discussed N-doped carbon with KOH activation via a calcination-induced self-assembly route, which exhibited a high SSA of 1538 $m^2/g$ and a $H_2S$-adsorption capacity of 10.5 mmol/g (0 °C, 1 kPas). N-6 is responsible for the improved $H_2S$-removal performance of N-doped carbon. Kan et al. (2019) also fabricated the N-doped ordered mesoporous carbon (N-OMCST-700) with KOH activation; however, the hydrothermally carbonized catalyst exhibited superior performance for the selective adsorption of $H_2S$ with an adsorption capacity of up to 13.4 mmol/g (0 °C, 1 bar). KOH activation of the catalyst increased the SSA (1575 $m^2/g$) and pore volume (0.52 $cm^3/g$). Such catalysts also exhibited a high N-content (4.46 wt%). DFT (Density Functional Theory) studies demonstrated strong interactions between the N-6 and N-5 sites. In addition, the basic surface nitrogen sites also participated in the dissociation of $H_2S$ to $HS^-$ and $H^+$, thus initiating the selective oxidation of $H_2S$ to elemental sulfur. Wu et al. (2022) described N-doped AC with a high N-content (17.2%) and a high meso-pore volume, which exhibited a high breakthrough sulfur capacity (1872 mg/g) for the catalytic oxidation of $H_2S$ under KOH activation. $K_2CO_3$ activation enhanced the SSA (from 187 to 2459 $m^2/g$) and total pore volume (from 0.255 to 1.453 $cm^3/g$) of the N-doped hierarchical carbon compared with those of N-doped and only $K_2CO_3$-activated porous carbon. It also exhibited excellent $H_2S$ removal with a sulfur capacity of 426.2 mg/g at room temperature compared to that shown by undoped porous carbon (i.e. 12.5 m/g); N-5 and N-6 acted as active sites for $H_2S$ adsorption (Chen et al. 2021). Chen et al. (2020) also highlighted the N-doped porous carbon (NPC) with a high SSA (1419 $m^2/g$) and total pore volume (0.80 $cm^3/g$); the $H_2S$-adsorption capacity (205.06 mg/g) is an obvious effect of $K_2CO_3$ activation over N-doped carbon prepared by hydrothermal carbonization. The hydrothermal temperature and duration helped increase the proportions of N-5 and N-6 in the porous carbon, which played a crucial role in $H_2S$ removal. The proposed mechanism for desulfurization using the NPC is detailed in Fig. 5. Chen et al. (2022) developed the N-doped interconnected mesoporous carbon with $H_2O_2$-assisted hydrothermal carbonization. $H_2O_2$ played a crucial role in $H_2S$ removal by forming a cross-linked mesoporous structure (the mesoporous volume increased from 0.01 to 0.31 $cm^3/g$) and increasing the numbers of abundant N-5 and N-6 sites. $H_2O_2$-activated N-doped carbon exhibited excellent $H_2S$-removal performance, with a $H_2S$-adsorption capacity of 181 mg/g, which was five times higher than that for obtained without $H_2O_2$ activation. Ma et al. (2021) reported N-doped carbon with an enhanced $H_2S$-adsorption capacity of 54.8 mg/g, higher SSA (1189 $m^2/g$), and larger total pore volume (0.433 $cm^3/g$) than those achieved using porous carbon without N-doping and

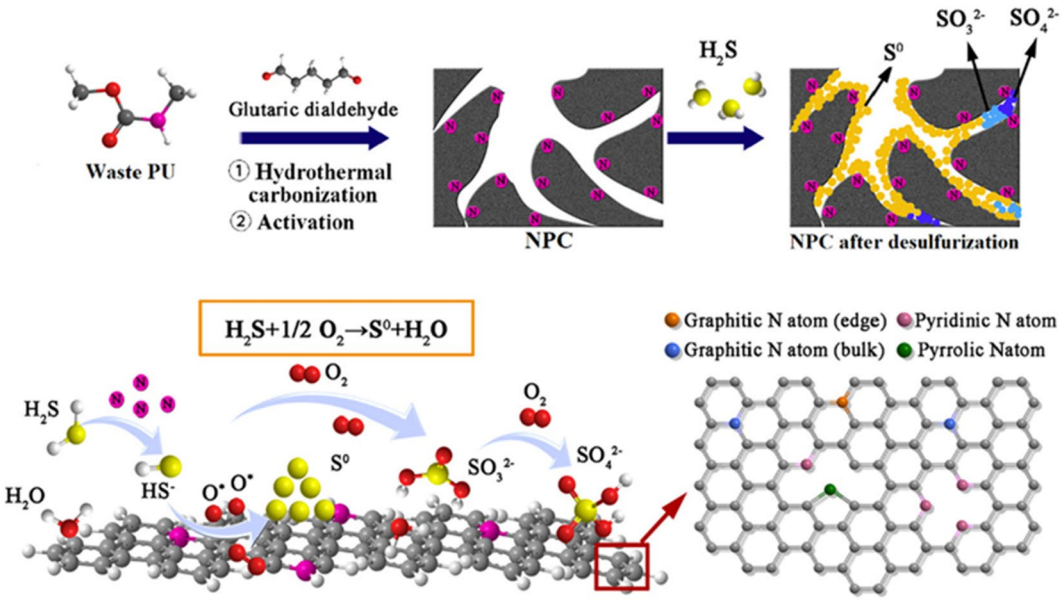


**Fig. 5** Schematic illustration showing $H_2S$ oxidation in the N-doped porous carbon (NPC) from waste PU (Chen et al. 2020)

activation. Among the N-containing groups, N-6 played a crucial role in $H_2S$ removal. Lei et al. (2023) reported a 3D cluster like the N-doped mesoporous carbon catalyst with a high SSA (330.5 $m^2/g$), hierarchical nanopores, and a large N-content (8.6%; where % N-6, N-5 > N-Q, i.e., > 60). Such catalysts exhibited 100% $H_2S$ conversion at 150 °C, with 94% sulfur selectivity. In addition, Ahmadi et al. (2021) highlighted that N-doping along with S-co-doping in carbon resulted in a high SSA (2579 $m^2/g$), large total pore volume (1.5 $cm^3/g$), and very high $H_2S$-adsorption capacity (17.19 mmol/g at 100 kPas). DFT studies confirmed the prominent role of N-5 in enhancing the adsorption energy of the molecules over the adsorbents. The S atom, as a codopant around the N-5 atom, controls the adsorption of $H_2S$ molecules with a lower adsorption energy, indicating that physisorption is more favorable than chemisorption. S co-doping (defects) plays a complementary role in controlling the adsorption mechanism of gas molecules. In addition, a higher S/N ratio results in better regeneration cycles. Thus, they established the source of novel electronic structures and, thereby, that of N-S-defected localities, both theoretically and experimentally.

## $Hg^0$ Removal

$Hg^0$ removal can be achieved through both physi-/chemisorption, which needs high surface area and porosity to produce more active sites. To improve the $Hg^0$-adsorption capacity, Liu et al. (2019) prepared seaweed-based novel ACs and demonstrated high $Hg^0$-adsorption capacity (2382.6 µg/g for SAC-800 and 2909.6 µg/g for EAC-800 catalyst) (Table 1). They demonstrated that an increase in the carbonization temperature enhances the SSA (from 399.57 to 524.57 $m^2/g$ in the SAC and from 339.04 to 565.82 $m^2/g$ in the EAC), with improved $Hg^0$-removal efficiency (from 40.4 to 88.9% in the SAC and from 34.25 to 90.7% in the EAC). The $Hg^0$-removal process involves both physisorption and chemisorption with suitable SSAs, pore structures, and functional moieties on the modified AC. Yang et al. (2018) also reported that the seaweed-based modified AC afforded an enhanced $Hg^0$-removal efficiency (91%). They revealed that the enhanced SSA (from 1.95 to 26.20 $m^2/g$) and $Hg^0$-removal performance (from 12 to 29.07%) were in line with those achieved at the increased carbonization temperature. Further chemical activation (using $NH_4Br$) decreased the surface area of the catalyst; however, it enhanced the $Hg^0$-removal efficiency, which is an obvious effect of the functional moieties (C–Br and C=O) serving as chemisorption sites. Li et al. developed a clean and modified method (a combination of microwave steam activation and $H_2O_2$ impregnation) to develop a porous carbon catalyst. The results suggest that microwave activation and $H_2O_2$ modification enhance the SSA (from to 154.92 to 433.03 $m^2/g$ in RSW10 and 108.80 to 273.91 $m^2/g$ in WSW10) and improve the pore structure (increase the pore volume from 0.217 to 0.2877 $cm^3/g$ in WSW10 and from 0.186 to 0.1860 $cm^3/g$ in RSW10) of the porous carbon (Li et al. 2021), which further facilitate the $Hg^0$-removal performance of the modified catalyst (i.e. 1293.19 µg/g for WSW10 and 1485.61 µg/g for RSW10) (see Table 1). Dou et al. described that $H_2O_2$ modification with UV improved the SSA of the modified AC (1408.61 $cm^3/g$), which further

enhanced its $Hg^0$-removal efficiency (from 61.71 to 90.04%). The maximum $Hg^0$-adsorption capacity was 3636.43 µg/g. $H_2O_2$ modification has a slight destructive effect on the pore structure; however, the significant increase in functional moieties (e.g.,–OH, C–O, and C=O) along with the chemisorbed oxygen (O*) enhances the mercury-removal performance of the catalyst. A schematic of the modification mechanism of AC using the UV/$H_2O_2$ advanced oxidation process (AOP) and the $Hg^0$-adsorption mechanism on the modified AC is shown in Fig. 6 (Dou et al. 2023). Liu et al. (2023b) reported a high $Hg^0$-adsorption capacity of 2052.51 µg/g for corn-stalk-based porous carbon developed by UV/$H_2O_2$ clean modification. Hence, it can be suggested that the SSA, pore volume, and functional moieties improve the $Hg^0$-removal performance of porous carbon catalysts. They also demonstrated that 3% of $H_2O_2$ is the critical concentration to achieve a high $Hg^0$-removal performance.

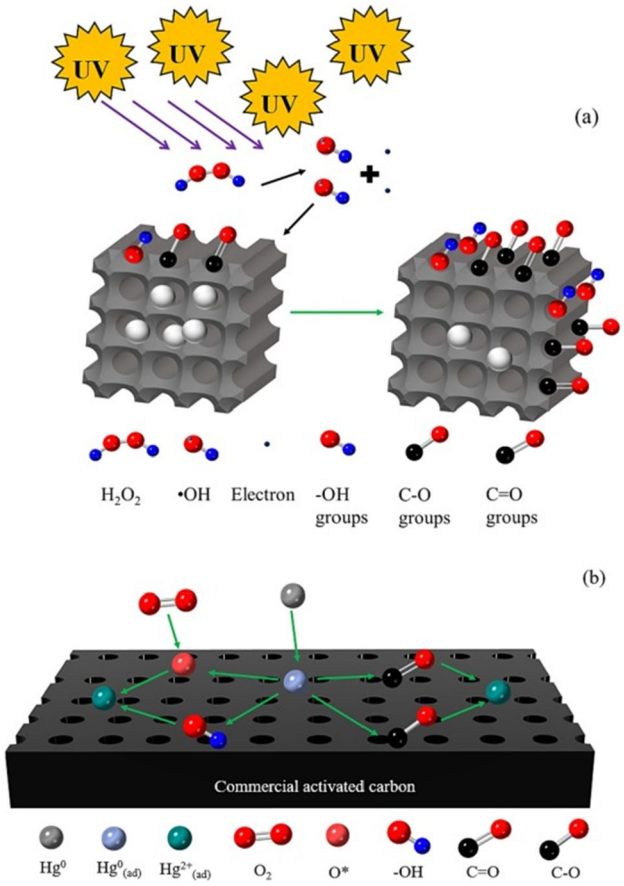


**Fig. 6** Schematic diagram of **a** modification of AC using UV/$H_2O_2$ advanced oxidation process (AOP) and **b** $Hg^0$ adsorption mechanism on the modified AC (Dou et al. 2023)

Wang et al. (2023a) reported a porous carbon catalyst prepared by secondary carbonation and activation with $K_2CO_3$, which showed SSA values as high as 2925 $m^2$/g and $Hg^0$-adsorption capacities as high as 571 mg/g. In addition, the $Hg^0$-removal performance remained stable for five consecutive adsorption–desorption cycles. A micromesoporous structure with fewer macropores greatly improves the $Hg^0$-adsorption capacity. The possible reaction pathways for $Hg^0$ adsorption onto the layered porous carbon (LPC) are shown in Fig. 7. Song et al. (2020) demonstrated the effects of carbonization temperature and KOH activation on the $Hg^0$-removal performance of anthracite-coal-based AC. They reported that the SSA increased (from 2.60 to 527.43 $m^2$/g) with increasing carbonization temperature and KOH activation, resulting in a catalyst with a better pore structure that afforded better $Hg^0$-removal performance. Li et al. (2015a) reported different solid-waste-based porous carbons developed using microwave and steam activation, which exhibited improved SSA, pore volume (especially micro), and $Hg^0$-removal efficiency (30–70%). Further impregnation with $NH_4Cl$ decreased the pore structure and surface area, although an enhanced $Hg^0$-adsorption capacity of 11,400 g/g was observed (Table 1). Wang et al. (2018a) reported HCl-modified porous carbon obtained

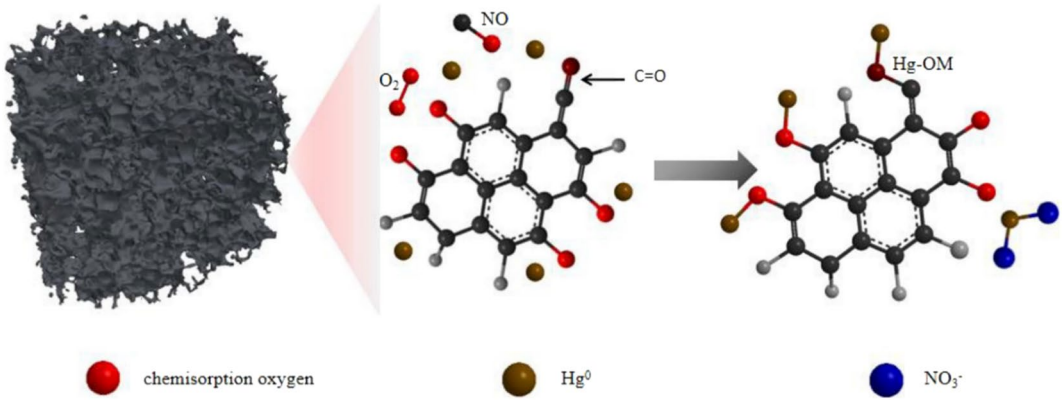


**Fig. 7** Possible reaction pathways of $Hg^0$ adsorption on layered porous carbon (LPC) (Wang et al. 2023a)

from various biochar sources with improved $Hg^0$ adsorption. The $Hg^0$-adsorption efficiency increased from 8.2 to 100% along with a better SSA (from 29.9 to 110.1 $m^2/g$); the macropores played a crucial role in this phenomenon.

Doping of porous carbon with metal oxides modifies its physicochemical properties, which can then be utilized to enhance the $Hg^0$ removal through adsorption and catalytic oxidation (Table 2). Gao et al. (2023) reported the effects of doping with metal and bimetal oxides on the $Hg^0$-removal efficiency of AC in a broad operating window (80–360 °C). Bimetal-oxide-doped AC (i.e., 6% $Co_{0.5}Cr_{0.5}$/AC) showed the optimal $Hg^0$-removal performance (88.3%) at 240 °C; in contrast, the use of undoped AC afforded only 40% $H_2S$ removal. This result shows the excellent tolerance of the doped catalyst to $SO_2$ and $H_2O$, which contributed to the redox cycle and synergistic effect between $CrO_x$ and $CoO_x$. Consequently, a large amount of sufficiently active $Co^{3+}$ species and surface-active oxygen were produced. In addition, the formation of a $CoCrO_4$ spinel was observed, which entailed the presence of abundant lattice defects, increment in the SSA and the number of active sites with a strong redox capacity, and a higher dispersion of active phases. Addition of $CoO_x$ to $CeO_2$-doped biomass AC (15% $Co_{0.4}Mn_{0.6}$/BAC) resulted in excellent $Hg^0$-removal efficiency (96.8%) at 230 °C through adsorption and catalytic oxidation, owing to the better texture, lower crystallinity, and strong redox ability of this AC. Moreover, the synergistic effect between $CoO_x$ and $CeO_x$ generated more $Ce^{3+}$ and $Co^{3+}$, inducing a large number of anionic defects and producing more active oxygen with oxygen vacancies (Gao et al. 2018). $CoO_x$-modified $MnO_x$-doped biomass AC afforded 98.5% $H_2S$-removal efficiency at 240 °C, which was higher than that achieved with undoped biomass AC (60%).

Addition of 15% $CoO_x$ to Mn-doped biomass AC contributed to the synergistic effect, which increased the SSA and $Mn^{4+}$ content, enhanced the redox ability and the strength, and restrained the $MnO_x$ crystallization, which might be responsible for the enhanced catalytic performance and $SO_2$ resistance of this catalyst (Gao et al. 2019). Yang et al. (2019) reported the effect of microwave steam treatment and iron-copper oxide doping on the wheat straw (WS)-derived carbon to improve the $Hg^0$-removal efficiency. The microwave steam treatment improved the $Hg^0$-removal efficiency of WS-derived carbon from 20 to 70% and further enhanced it to 90.58% (2276.45 μg/g of $Hg^0$-adsorption capacity) in CuFe0.3/WSWU10(500) at 130 °C owing to Cu-Fe oxide doping. The Cu-Fe active phases, chemisorbed oxygen, and lattice oxygen play crucial roles in the removal of $Hg^0$. Chemisorption is the key rate-controlling step. Zhang et al. (2021) discussed the promotional effect of $FeO_x$ and the doping effect of $MnO_x$ on a biochar-based composite prepared by ball milling for $Hg^0$ removal. The MnFe/char-BM4 catalyst exhibited > 95% $Hg^0$-removal efficiency at 100 °C through the physical adsorption and catalytic oxidation mechanism.

Heteroatom doping (with N, S, and P) is an effective method for modifying carbon sorbents and improving their chemical reactivity for $Hg^0$ removal (Table 3). Zhou et al. (2022a) discussed the P-doped biochar ($PBC_{900}$) without any additional modification, which exhibited a high SSA (1038.34 $m^2/g$) and large $Hg^0$ adsorption (15,047.64 μg/g); in contrast, undoped BC (BC900) showed an SSA of 394.86 $m^2/g$ and a $Hg^0$-adsorption capacity of 36.58 μg/g. In addition, more organic functional groups were generated on the PBC surface, such as C-O=P and C=O. With these groups, the O-C=O group can serve as an electron acceptor, accelerating the electron-migration process for $Hg^0$ oxidization. Zhou et al. (2022b) reported S-doped mesoporous carbon (SMC-900), which exhibited a high SSA (993 $m^2/g$) and excellent $Hg^0$-removal performance (> 97% at 50–150 °C) and discussed the effects of the precursor ratio and carbonization on the mercury-removal performance. The sulfur was in the form of thiophene (C-S-C) and oxidized sulfur (C-$SO_x$-C), and the S-content was 10.29%. However, Vakili et al. (2021) highlighted that the N- and S-doped nanoporous carbon (NSDG-10) exhibited the highest $Hg^0$-removal performance (94.5%), whereas that for unmodified or non-doped carbon was 71%. These results indicate that high SSA and pore volume did not contribute significantly to high mercury adsorption because the N- and S-doped carbon showed better $Hg^0$ removal despite having a lower SSA and a smaller pore volume.

## VOC (Toluene) Removal

Physically and chemically activated carbon can also be used for removing toluene. Mohammed et al. (2015) reported a toluene-adsorption capacity of 238.10 mg/g for coconut-shell-based AC with KOH activation. Further, the ammonia-treated AC (PHAC-AM) catalyst exhibited a decreased surface area (from 478 to 361.8 $m^2/g$) and a reduced total pore volume (from 0.61 to 0.16 $cm^3/g$). However, the toluene-adsorption capacity enhanced by 10%, i.e., 357.14 mg/g. Ammonia treatment increases the number of basic surface functional groups, which further improves the affinity of AC for VOCs. Li et al. (2020a) reported a sodium lignin sulfonate-based carbon catalyst with very high toluene adsorption (> 2300 mg/g); the porous carbon was activated by metal salts. Among them, $ZnCl_2$-activated porous carbon exhibited the highest SSA (1524 $m^2/g$) and mesopore volume (1092 $m^2/g$), which facilitated VOC adsorption. In addition, many functional groups play crucial roles in enhancing the toluene adsorption. Highly porous carbon with a toluene-adsorption capacity of 1587 mg/g and an extremely high surface area (4293 $m^2/g$) was developed using waste soybean residues with pre-carbonization, KOH activation,

and pyrolysis. The activation temperature and KOH dosage affected the SSA and total pore volume (mesopores and micropores). Porous carbon exposes the aromatic sites (e.g., phenol) for π–π interaction with toluene. Presence of metallic K in porous carbon causes extensive intercalation at the surface of graphitic microcrystals, which exposes the microscale space. The exposed aromatic π system may interact with toluene molecules through strong π–π stacking (Li et al. 2022a). Overall, the SSA, pore volume, and functional moieties play key roles in enhancing the toluene-removal rate.

Metal-doped porous carbon can also be utilized to remove toluene by modifying its physicochemical properties (Lei et al. 2020; Li et al. 2020b). The CuO-doped AC exhibited a toluene-adsorption capacity of 701.8 mg/g at 20 °C. CuO doping mainly increases the pore size, which facilitates the migration and diffusion of toluene and improves its adsorption (Lei et al. 2020). Li et al. (2020b) reported the $CuCo_{0.5}$/C catalyst with better performance, i.e., 90% toluene removal at 243 °C, owing to a large SSA, more chemisorbed active oxygen species, and a high ratio of $Co^{2+}/Co^{3+}$.

Toluene removal can also be achieved by using heteroatom-doped modified porous carbon. In particular, the NPC enhanced the surface charge distribution and activity of carbon, which further enhanced the adsorption performance for toluene removal (Table 3). Jin et al. (2022a) developed N-doped porous carbon (NPC-1) with an ultrahigh SSA (3235 $m^2$/g) and total pore volume (2 $cm^3$/g), exhibiting a higher adsorption capacity (691.1 mg/g) compared to those reported previously (Fig. 8), which originated from the use of an alkali metal activator (KOH) and an N-dopant (urea). NPC-1 showed a three-dimensional pore structure. Micropore filling is the main mechanism of toluene adsorption. DFT analysis revealed that N-6, as an active site, promoted the adsorption capacity through an interaction mechanism. Cheng et al. (2023) also reported the effect of N-doping and activators on improving the pore structure, increasing the SSA (1000 $m^2$/g), and enhancing the toluene-adsorption capacity (223 mg/g), which maintained 80% adsorption capacity under humid conditions. Besides, a DFT study revealed the dependency

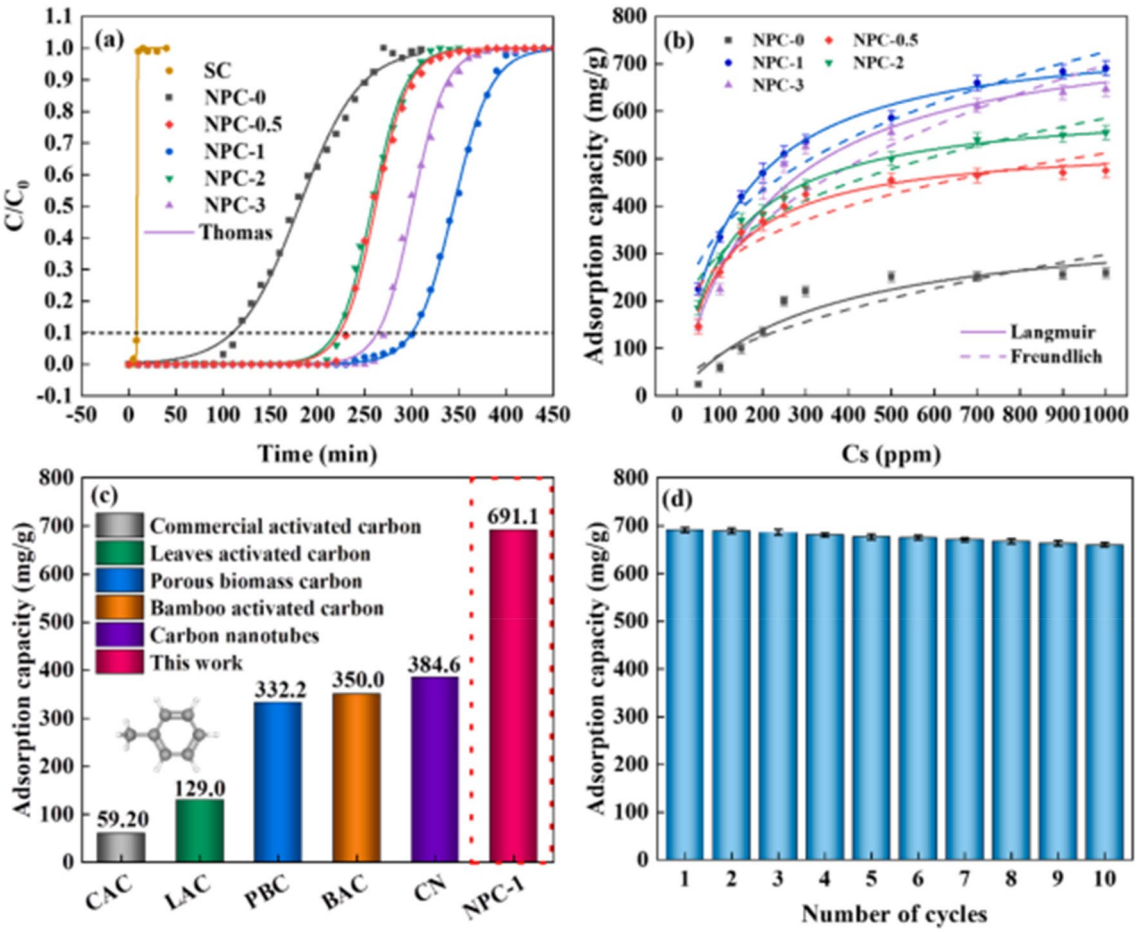


**Fig. 8** Toluene-adsorption property of NPCs (N-doped porous carbon): **a** Breakthrough curves for toluene, **b** adsorption isotherms, **c** comparison of adsorption capacity of similar carbon materials, and **d** cyclic performance of NPCs (Jin et al. 2022a)

of N-containing functional groups over the π–π dispersion and hydrophobic and electrostatic interactions, which promote toluene adsorption. Figure 9 shows the selective adsorption mechanism of toluene on the amino-functionalized modified carbon under humid conditions. Xu et al. (2021) reported the N-doped carbon with good performance for the adsorption of toluene (720 mg/g) and high SSA (2060 $m^2$/g). A DFT study revealed that a large number of amino functional groups (3.6%) exhibited highly strong affinity for toluene than that for N-6, N-5, and so on. Biomass-derived N-doped hierarchical porous carbon (NHPC) exhibited a large SSA (2266 $m^2$/g), a high pore volume (1.14 $cm^3$/g), and a particularly high toluene adsorption (5.94 mmol/g), while corncob-derived N-doped carbon with a higher total cellulose content and lower ash content resulted in a better pore activation effect (Huang et al. 2023). Du et al. (2020) reported an N–O co-doped hierarchical carbon material with a high SSA (1650 $m^2$/g) and toluene-adsorption capacity (627 mg/g), where the hierarchical porosity and high SSA were the key factors for physical adsorption. N-containing functional moieties significantly enhanced the chemical adsorption, while N-5 exhibited the highest affinity for toluene molecules. Shi et al. (2022a) reported N–O co-doped porous carbon with a high SSA (2784.53 $m^2$/g), a hierarchical pore structure, high N (16.16%) and O (15.75%) contents, and excellent toluene adsorption (813.6 mg/g). DFT studies revealed that the interaction among the toluene molecules can be improved by N–O functional groups and multilayer adsorption can be achieved, wherein the optimal adsorption pore size of the N–O co-doped porous carbon was 3–7 times the dynamic diameter of toluene. These optimal adsorption pores provide pathways and adsorption sites that allow the highest adsorption capacity of toluene.

## Conclusions

Different strategies have been developed to improve the air-pollutant-removal performance of carbon-based catalysts, such as physical or chemical treatment/activation, metal oxide doping, and heteroatom doping. In physical treatment, $CO_2$ and steam played a major role in controlling the surface properties (such as SSA, pore size distribution, and pore volume), which further enhanced the removal of toxic gases/pollutants ($NO_x$, $H_2S$, $Hg^0$, and toluene). Chemical treatment/activation (with acid or alkaline salts) provides more functional moieties with an improved pore structure and SSA, which enhance the adsorption of porous carbon (particularly, the adsorption capacity of $H_2S$, $Hg^0$, and toluene). In addition, carbonization and calcination temperatures affect the pore structure of carbon-based catalysts, which is important for reactive gas adsorption during catalysis.

Metal oxide doping enhances the surface acidity and redox ability of the catalyst, which in turn enhances the SCR of $NO_x$ and poisoning tolerance. Moreover, pre- and/or post-oxidation of the catalyst helps in improving the surface and structural properties of carbon. Co-doping with metal oxides increases the catalytic performance by broadening the reaction window and resisting poisoning. In addition, metal oxide doping with acid/base modification (i.e., oxygen functionalization/surface modification) provides high $SO_2$/$H_2O$ tolerance to catalyst poisoning and enhances the catalytic performance. The basicity and synergistic effect of the carbon catalyst also help improve the $H_2S$-adsorption capacity, wherein the calcination temperature and activation play a crucial role. For $Hg^0$ adsorption, metal oxide doping provides more active oxygen and vacancies, better redox strength, and a synergistic effect, which are beneficial for pollutant adsorption and oxidation. The enlarged pore size with increased SSA and active chemisorbed oxygen due to

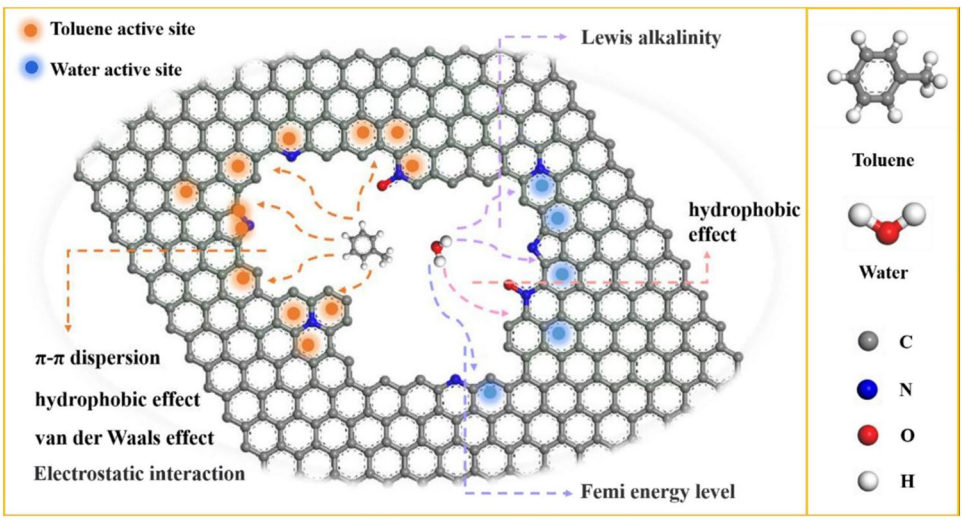


**Fig. 9** Selective adsorption mechanism of toluene on amino-functionalized modified biochar under humid conditions (Cheng et al. 2023)

metal oxide doping enhance the toluene-adsorption capacity of the carbon catalyst.

Heteroatom doped (N/S) carbon-based single-atom carbon leads to enhance the high stability, catalytic reaction, and/or electrocatalysis activity. Regulating the electronic structure of N-doped carbon metal catalyst at atomic level effectively enhances the catalytic activity. Heteroatom doping (with N, O, S/P, and B) plays a critical role in enhancing the catalytic properties of porous carbon. In particular, the N-content with unpaired electrons is crucial for enhancing the adsorption and oxidation of NO and $NH_3$ because of the abundant Lewis acid sites that promote the SCR of NO. In addition, the N-containing functional groups (especially N-6) play a significant role in promoting the SCR performance of the carbon catalyst. The synergistic effect of dual heteroatom dopants (N and O) enhances the carbon-catalyzed $NH_3$ SCR of $NO_x$. The basic surface nitrogen sites (N-6 and N-5) also participate in the dissociation of $H_2S$ to $HS^-$ and $H^+$, thus initiating the selective oxidation of $H_2S$ to elemental sulfur. N and S co-doping along with $H_2O_2$ hydrothermal treatment improve the SSA and pore volume, which have a significant effect on the $H_2S$-adsorption capacity of the carbon catalyst with a high N-5 content. P- and S-doped carbon materials enhance the SSA and pore volume, leading to high $Hg^0$ adsorption. However, this is not the case for N- and S-co-doped carbon. In addition, the activator significantly enhances toluene adsorption with a modified carbon catalyst.

After exploring the development of carbon catalysts with various modifications, the following conclusions can be drawn:

1. Development of new precursor materials can be explored for producing carbon catalysts with enhanced gas-pollutant (multipollutant)-removal efficiency, thereby strengthening the anti-poisoning and mechanical properties through commercialization.
2. As the environmental concerns are attracting increasing attention, new activation methods that use renewable energy sources or develop closed-loop systems for carbon recovery and reuse are being explored.
3. Designing heteroatom-doped carbon catalysts with tailored properties and functionalities can help optimize their performances for specific applications. This may improve our understanding of the structure–property relationships of these catalysts. Further research efforts are required to optimize their performance and reduce costs for widespread commercial adoption of such catalysts.
4. In-depth understanding of the mechanisms involved in the catalytic activity of carbon materials is required.
5. A recovery method for used carbon catalysts is needed to conserve the valuable resources.

**Acknowledgements** This research was financially supported by Basic Science Research Program through the National Research Foundation of Korea (NRF) funded by the Ministry of Education (2021R1I1A3050146 & RS-2023-00249553), the Ministry of Science and ICT (MSIT) (No. RS-2023-00218203), and Korea Ministry of Environment (MOE) as Waste to energy recycling Human resource development Project.

**Author contributions** Jae Hwan Yang: Conceptualization, review, editing, and supervision. Ajit Dattatray Phule: Conceptualization, writing-original draft preparation, writing-review and editing. Md. Wahad Uz Zaman: writing-review and editing. Sahar Elkaee: writing-review and editing. Seul Yi Kim: writing-review and editing. Sang Gyu Lee: writing-review and editing. Gibeom Park: writing-review and editing. All authors have read and agreed to the published version of the manuscript.

**Funding** This research was financially supported by Basic Science Research Program through the National Research Foundation of Korea (NRF) funded by the Ministry of Education (2021R1I1A3050146 & RS-2023-00249553), the Ministry of Science and ICT (MSIT) (No. RS-2023-00218203), and Korea Ministry of Environment (MOE) as Waste to energy recycling Human resource development Project.

**Data availability** The authors have included all the relevant data and the source of freely available data in the manuscript.

## Declarations

**Conflict of interest** The authors declare that they have no known competing financial or non-financial interest that could have appeared to influence the work reported in this paper.

## References

Ahmadi R, Alivand MS, Haj Mohammad Hossein Tehrani N, Ardjmand M, Rashidi A, Rafizadeh M, Seif A, Mollakazemi F, Noorpoor Z, Rudd J (2021) Preparation of fiber-like nanoporous carbon from jute thread waste for superior $CO_2$ and $H_2S$ removal from natural gas: experimental and DFT study. Chem Eng J 415:129076. https://doi.org/10.1016/j.cej.2021.129076

Anthonysamy SBI, Afandi SB, Khavarian M, Mohamed ARB (2018) A review of carbon-based and non-carbon-based catalyst supports for the selective catalytic reduction of nitric oxide. Beilstein J Nanotechnol 9:740–761. https://doi.org/10.3762/bjnano.9.68

Bai X, Han J, Niu X, Guan J (2023a) The d-orbital regulation of isolated manganese sites for enhanced oxygen evolution. Nano Res 16:10796–10802. https://doi.org/10.1007/s12274-023-5859-8

Bai X, Wang Y, Han J, Niu X, Guan J (2023b) Engineering the electronic structure of isolated manganese sites to improve the oxygen reduction, Zn-air battery and fuel cell performances. Appl Catal B Environ 337:122966. https://doi.org/10.1016/j.apcatb.2023.122966

Balsamo M, Cimino S, de Falco G, Erto A, Lisi L (2016) ZnO-CuO supported on activated carbon for H2S removal at room temperature. Chem Eng J 304:399–407. https://doi.org/10.1016/j.cej.2016.06.085

Bazan-Wozniak A, Nowicki P, Pietrzak R (2017) The influence of activation procedure on the physicochemical and sorption properties of activated carbons prepared from pistachio nutshells for removal of $NO_2$ /$H_2S$ gases and dyes. J Clean Prod 152:211–222. https://doi.org/10.1016/j.jclepro.2017.03.114

Chen W, Zhang G, Li D, Ma S, Wang B, Jiang X (2020) Preparation of nitrogen-doped porous carbon from waste polyurethane foam by hydrothermal carbonization for $H_2S$ adsorption. Ind Eng Chem Res 59:7447–7456. https://doi.org/10.1021/acs.iecr.0c00498

Chen L, Yuan J, Li T, Jiang X, Ma S, Cen W, Jiang W (2021) A regenerable N-rich hierarchical porous carbon synthesized from waste biomass for $H_2S$ removal at room temperature. Sci Total Environ 768:144452. https://doi.org/10.1016/j.scitotenv.2020.144452

Chen L, Jiang X, Chen W, Dai Z, Wu J, Ma S, Jiang W (2022) $H_2O_2$-assisted self-template synthesis of N-doped biochar with interconnected mesopore for efficient $H_2S$ removal. Sep Purif Technol 297:121410. https://doi.org/10.1016/j.seppur.2022.121410

Cheng T, Bian Y, Li J, Ma X, Yang L, Zhou L, Wu H (2023) Nitrogen-doped porous biochar for selective adsorption of toluene under humid conditions. Fuel 334:126452. https://doi.org/10.1016/j.fuel.2022.126452

Chiang Y-C, Chiang P-C, Huang C-P (2001) Effects of pore structure and temperature on VOC adsorption on activated carbon. Carbon 39:523–534

Cho S-H, Lee S, Kim Y, Song H, Lee J, Tsang YF, Chen W-H, Park Y-K, Lee D-J, Jung S, Kwon EE (2023) Applications of agricultural residue biochars to removal of toxic gases emitted from chemical plants: A review. Sci Total Environ 868:161655. https://doi.org/10.1016/j.scitotenv.2023.161655

Cui S, Zhao Y, Liu Y, Pan J (2022) Preparation of copper-based biochar adsorbent with outstanding $H_2S$ adsorption capacity and study on $H_2S$ removal. J Energy Inst 105:481–490. https://doi.org/10.1016/j.joei.2022.11.004

Damma D, Ettireddy P, Reddy B, Smirniotis P (2019) A review of low temperature $NH_3$-SCR for removal of NOx. Catalysts 9:349. https://doi.org/10.3390/catal9040349

de Falco G, Montagnaro F, Balsamo M, Erto A, Deorsola FA, Lisi L, Cimino S (2018) Synergic effect of Zn and Cu oxides dispersed on activated carbon during reactive adsorption of $H_2S$ at room temperature. Microporous Mesoporous Mater 257:135–146. https://doi.org/10.1016/j.micromeso.2017.08.025

Dou Z, Wang Y, Liu Y, Zhao Y, Huang R (2023) Enhanced adsorption of gaseous mercury on activated carbon by a novel clean modification method. Sep Purif Technol 308:122885. https://doi.org/10.1016/j.seppur.2022.122885

Du Y, Chen H, Xu X, Wang C, Zhou F, Zeng Z, Zhang W, Li L (2020) Surface modification of biomass derived toluene adsorbent: hierarchically porous characterization and heteroatom doped effect. Microporous Mesoporous Mater 293:109831. https://doi.org/10.1016/j.micromeso.2019.109831

Fang H, Zhao J, Fang Y, Huang J, Wang Y (2013) Selective oxidation of hydrogen sulfide to sulfur over activated carbon-supported metal oxides. Fuel 108:143–148. https://doi.org/10.1016/j.fuel.2011.05.030

Fidalgo B, Menéndez JÁ (2011) Carbon materials as catalysts for decomposition and $CO_2$ reforming of methane: a review. Chin J Catal 32:207–216. https://doi.org/10.1016/S1872-2067(10)60166-0

Gao L, Li C, Zhang J, Du X, Li S, Zeng J, Yi Y, Zeng G (2018) Simultaneous removal of NO and $Hg^0$ from simulated flue gas over CoOx -$CeO_2$ loaded biomass activated carbon derived from maize straw at low temperatures. Chem Eng J 342:339–349. https://doi.org/10.1016/j.cej.2018.02.100

Gao L, Li C, Li S, Zhang W, Du X, Huang L, Zhu Y, Zhai Y, Zeng G (2019) Superior performance and resistance to $SO_2$ and $H_2O$ over CoOx-modified MnOx/biomass activated carbons for simultaneous $Hg^0$ and NO removal. Chem Eng J 371:781–795. https://doi.org/10.1016/j.cej.2019.04.104

Gao L, Yi L, Xie D, Wang H, Li C, Li L, Liu Y, Xie J, Zhou Y, Liu Y (2023) Insight into the design and construction of Cr substituted Co-based columnar activated coke catalysts for effective and reliable removal of methylbenzene and $Hg^0$ concurrently. Fuel 334:126732. https://doi.org/10.1016/j.fuel.2022.126732

Guo J, Luo Y, Lua AC, Chi R, Chen Y, Bao X, Xiang S (2007) Adsorption of hydrogen sulphide ($H_2S$) by activated carbons derived from oil-palm shell. Carbon 45:330–336. https://doi.org/10.1016/j.carbon.2006.09.016

Guo F, Huang X, Chen Z, Sun H, Shi W (2020) Investigation of visible-light-driven photocatalytic tetracycline degradation via carbon dots modified porous $ZnSnO_3$ cubes: Mechanism and degradation pathway. Sep Purif Technol 253:117518. https://doi.org/10.1016/j.seppur.2020.117518

Gupta VK, Saleh TA (2013) Sorption of pollutants by porous carbon, carbon nanotubes and fullerene- an overview. Environ Sci Pollut Res 20:2828–2843. https://doi.org/10.1007/s11356-013-1524-1

Huang B, Huang R, Jin D, Ye D (2007) Low temperature SCR of NO with $NH_3$ over carbon nanotubes supported vanadium oxides. Catal Today 126:279–283. https://doi.org/10.1016/j.cattod.2007.06.002

Huang X, Tang M, Li H, Wang L, Lu S (2023) Adsorption of multicomponent VOCs on various biomass-derived hierarchical porous carbon: a study on adsorption mechanism and competitive effect. Chemosphere 313:137513. https://doi.org/10.1016/j.chemosphere.2022.137513

Jia X et al (2022) Lotus leaves-derived MnOx/biochar as an efficient catalyst for low-temperature $NH_3$-SCR removal of NOx: effects of modification methods of biochar. J Chem Technol Biotechnol 97:3100–3110

Jiang L, Liu Q, Ran G, Kong M, Ren S, Yang J, Li J (2019) $V_2O_5$-modified Mn-Ce/AC catalyst with high $SO_2$ tolerance for low-temperature $NH_3$-SCR of NO. Chem Eng J 370:810–821. https://doi.org/10.1016/j.cej.2019.03.225

Jin B, Li J, Wang Y, Yang Z, Yao X, Sun W, Lu Y, Zhu X, Zhang T (2022a) Nitrogen doping and porous tuning carbon derived from waste biomass boosting for toluene capture: experimental study and density functional theory simulation. Chem Eng J Adv 10:100276. https://doi.org/10.1016/j.ceja.2022.100276

Jin Y, Ding S, Li P, Wang X (2022b) Coordination of thin-film nanofibrous composite dialysis membrane and reduced graphene oxide aerogel adsorbents for elimination of indoxyl sulfate. Chin J Chem Eng 49:111–121. https://doi.org/10.1016/j.cjche.2022.01.024

Kan X, Chen X, Chen W, Mi J, Zhang J-Y, Liu F, Zheng A, Huang K, Shen L, Au C, Jiang L (2019) Nitrogen-decorated, ordered mesoporous carbon spheres as high-efficient catalysts for selective capture and oxidation of $H_2S$. ACS Sustain Chem Eng 7:7609–7618. https://doi.org/10.1021/acssuschemeng.8b05852

Kim et al (2018) Development of high performance catalytic filter of $V_2O5$-$WO_3$/$TiO_2$ supported-SiC for NOx reduction. Powder Technol 327:282–290

Ku BJ, Lee JK, Park D, Rhee H-K (1994) Treatment of activated carbon to enhance catalytic activity for reduction of nitric oxide with ammonia. Ind Eng Chem Res 33:2868–2874. https://doi.org/10.1021/ie00035a042

Lei B, Liu B, Zhang H, Yan L, Xie H, Zhou G (2020) CuO-modified activated carbon for the improvement of toluene removal in air. J Environ Sci 88:122–132. https://doi.org/10.1016/j.jes.2019.07.001

Lei G, Fan Z, Hou Y, Liu F, Wang S, Shen L, Zhan Y, Jiang L (2023) Facile template-free synthesis of 3D cluster-like nitrogen-doped mesoporous carbon as metal-free catalyst for selective oxidation of $H_2S$. J Environ Chem Eng 11:109095. https://doi.org/10.1016/j.jece.2022.109095

Li Q, Hou Y, Han X, Huang Z, Guo Q, Sun D, Liu J (2014) Selective catalytic reduction of NO with $NH_3$ over activated carbon impregnated with melamine at low temperature. J Fuel Chem

Technol 42:487–493. https://doi.org/10.1016/S1872-5813(14)60025-6
Li G, Shen B, Wang Y, Yue S, Xi Y, An M, Ren K (2015a) Comparative study of element mercury removal by three bio-chars from various solid wastes. Fuel 145:189–195. https://doi.org/10.1016/j.fuel.2014.12.083
Li W, Tan S, Shi Y, Li S (2015b) Utilization of sargassum based activated carbon as a potential waste derived catalyst for low temperature selective catalytic reduction of nitric oxides. Fuel 160:35–42. https://doi.org/10.1016/j.fuel.2015.07.045
Li B, Xiong H, Xiao Y, Hu J, Zhang X, Li L, Wang R (2020a) Efficient toluene adsorption on metal salt-activated porous carbons derived from low-cost biomass: a discussion of mechanism. ACS Omega 5:13196–13206. https://doi.org/10.1021/acsomega.0c01230
Li J-R, Wang F-K, He C, Huang C, Xiao H (2020b) Catalytic total oxidation of toluene over carbon-supported Cu Co oxide catalysts derived from Cu-based metal organic framework. Powder Technol 363:95–106. https://doi.org/10.1016/j.powtec.2019.12.060
Li Q, Hou Y, Wang J, Liu Y, Xiang N, Huang Z (2020c) Superiority of raw biomass and potassium hydroxide in preparation of ultrahigh nitrogen doping of carbon for $NH_3$-SCR reaction. ACS Sustain Chem Eng 8:11308–11316. https://doi.org/10.1021/acssuschemeng.0c03193
Li Q, Hou Y, Xiang N, Liu Y, Huang Z (2020d) A new insight into the promotional effect of nitrogen-doping in activated carbon for selective catalytic reduction of $NO_X$ with $NH_3$. Sci Total Environ 740:140158. https://doi.org/10.1016/j.scitotenv.2020.140158
Li W, Jin S, Zhang R, Wei Y, Wang J, Yang S, Wang H, Yang M, Liu Y, Qiao W, Ling L, Jin M (2020e) Insights into the promotion role of phosphorus doping on carbon as a metal-free catalyst for low-temperature selective catalytic reduction of NO with $NH_3$. RSC Adv 10:12908–12919. https://doi.org/10.1039/D0RA01654C
Li Y, Liu Y, Yang W, Liu L, Pan J (2021) Adsorption of elemental mercury in flue gas using biomass porous carbons modified by microwave/hydrogen peroxide. Fuel 291:120152. https://doi.org/10.1016/j.fuel.2021.120152
Li D, Yang J, Zhao Y, Yuan H, Chen Y (2022a) Ultra-highly porous carbon from Wasted soybean residue with tailored porosity and doped structure as renewable multi-purpose absorbent for efficient $CO_2$, toluene and water vapor capture. J Clean Prod 337:130283. https://doi.org/10.1016/j.jclepro.2021.130283
Li Q, Liang M, Han X, Hou Y, Huang Z (2022b) Insight into the enhancing activity and stability of Ce modified $V_2O_5$/AC during cyclic desulfurization-regeneration-denitrification. J Hazard Mater 424:127397. https://doi.org/10.1016/j.jhazmat.2021.127397
Li Y, Yu J, Liu Y, Huang R, Wang Z, Zhao Y (2022c) A review on removal of mercury from flue gas utilizing existing air pollutant control devices (APCDs). J Hazard Mater 427:128132. https://doi.org/10.1016/j.jhazmat.2021.128132
Li S, Huang Y, Zhu H, Long J, Xiao L, Li P, Zhao L, Zhang J (2023a) Dual improvement in acid and redox properties of the FeO/OAC catalyst via APS oxygen-functionalization: high low-temperature NH3-SCR activity, $SO_2$ and $H_2O$ tolerance. Fuel 341:127716. https://doi.org/10.1016/j.fuel.2023.127716
Li X, Sun F, Qu Z, Zhu X, Gao J, Zhao G, Zhang L (2023b) Insight into synergistic effects of oxygen and nitrogen dual-dopants in carbon catalysts on selective catalytic reduction of NOx with $NH_3$: a combined computational and experimental verification. Chem Eng J 454:140098. https://doi.org/10.1016/j.cej.2022.140098
Li Y, Wang Y, Dou Z, Liu Y (2023c) Removal of gaseous Hg0 using biomass porous carbons modified by an environmental-friendly photochemical technique. Chem Eng J 457:141152. https://doi.org/10.1016/j.cej.2022.141152
Liang S, Mi J, Liu F, Zheng Y, Xiao Y, Cao Y, Jiang L (2020) Efficient catalytic elimination of COS and $H_2S$ by developing ordered mesoporous carbons with versatile base N sites via a calcination induced self-assembly route. Chem Eng Sci 221:115714. https://doi.org/10.1016/j.ces.2020.115714
Lin Y, Li Y, Xu Z, Xiong J, Zhu T (2018) Transformation of functional groups in the reduction of NO with $NH_3$ over nitrogen-enriched activated carbons. Fuel 223:312–323. https://doi.org/10.1016/j.fuel.2018.01.092
Liu Z, Adewuyi YG, Shi S, Chen H, Li Y, Liu D, Liu Y (2019) Removal of gaseous $Hg^0$ using novel seaweed biomass-based activated carbon. Chem Eng J 366:41–49. https://doi.org/10.1016/j.cej.2019.02.025
Liu L, Wang B, Yao X, Yang L, Jiang W, Jiang X (2021) Highly efficient MnOx/biochar catalysts obtained by air oxidation for low-temperature $NH_3$-SCR of NO. Fuel 283:119336. https://doi.org/10.1016/j.fuel.2020.119336
Liu S, Feng X, Liu Z, Zhao W, Li Y, Zhang J (2023a) Nitrogen doping in porous biochar from cotton stalk with $H_3PO_4$ activation for reduction of NOx with $NH_3$-SCR at low temperatures: Characteristics and catalytic activity analysis. Fuel 332:126256. https://doi.org/10.1016/j.fuel.2022.126256
Liu Y, Cui S, Wu P, Liu L, Dou Z, Wang Y (2023b) Removal of gaseous elemental mercury using corn stalk biochars modified by a green oxidation technology. Fuel Process Technol 242:107621. https://doi.org/10.1016/j.fuproc.2022.107621
Ma Z, Zhang H, Yang Z, Ji G, Yu B, Liu X, Liu Z (2016) Mesoporous nitrogen-doped carbons with high nitrogen contents and ultrahigh surface areas: synthesis and applications in catalysis. Green Chem 18:1976–1982. https://doi.org/10.1039/C5GC01920F
Ma Q, Chen W, Jin Z, Chen L, Zhou Q, Jiang X (2021) One-step synthesis of microporous nitrogen-doped biochar for efficient removal of $CO_2$ and $H_2S$. Fuel 289:119932. https://doi.org/10.1016/j.fuel.2020.119932
Mohammed J, Nasri NS, Ahmad Zaini MA, Hamza UD, Ani FN (2015) Adsorption of benzene and toluene onto KOH activated coconut shell based carbon treated with $NH_3$. Int Biodeterior Biodegrad 102:245–255. https://doi.org/10.1016/j.ibiod.2015.02.012
Murindababisha D, Yusuf A, Sun Y, Wang C, Ren Y, Lv J, Xiao H, Chen GZ, He J (2021) Current progress on catalytic oxidation of toluene: a review. Environ Sci Pollut Res 28:62030–62060. https://doi.org/10.1007/s11356-021-16492-9
Nicolae SA, Louis-Therese J, Gaspard S, Szilágyi PÁ, Titirici MM (2022) Biomass derived carbon materials: synthesis and application towards $CO_2$ and $H_2S$ adsorption. Nano Sel 3:165–177. https://doi.org/10.1002/nano.202100099
Pan J, Wang L, Shi Y, Li L, Xu Z, Sun H, Guo F, Shi W (2022) Construction of nanodiamonds/UiO-66-$NH_2$ heterojunction for boosted visible-light photocatalytic degradation of antibiotics. Sep Purif Technol 284:120270. https://doi.org/10.1016/j.seppur.2021.120270
Panwar NL, Pawar A (2022) Influence of activation conditions on the physicochemical properties of activated biochar: a review. Biomass Convers Biorefin 12:925–947. https://doi.org/10.1007/s13399-020-00870-3
Rubel AM, Stencel JM (1997) The effect of low-concentration $SO_2$ on the adsorption of NO from gas over activated carbon. Fuel 76:521–526. https://doi.org/10.1016/S0016-2361(96)00221-9
Shi W, Shi C, Sun W, Liu Y, Guo F, Lin X (2021) Dual enhancement of photooxidation and photoreduction activity by coating CdS nanoparticles on lignin-based biomass carbon with irregular flower-like structure. J Mater Sci 56:19452–19465. https://doi.org/10.1007/s10853-021-06589-4
Shi R, Liu K, Liu B, Chen H, Xu X, Ren Y, Qiu J, Zeng Z, Li L (2022a) New insight into toluene adsorption mechanism of melamine urea-formaldehyde resin based porous carbon: experiment

and theory calculation. Colloids Surf Physicochem Eng Asp 632:127600. https://doi.org/10.1016/j.colsurfa.2021.127600
Shi W, Hao C, Fu Y, Guo F, Tang Y, Yan X (2022b) Enhancement of synergistic effect photocatalytic/persulfate activation for degradation of antibiotics by the combination of photo-induced electrons and carbon dots. Chem Eng J 433:133741. https://doi.org/10.1016/j.cej.2021.133741
Shi W, Liu Y, Sun W, Hong Y, Li X, Lin X, Guo F, Shi J (2022c) Improvement of synergistic effect photocatalytic/peroxymonosulfate activation for degradation of amoxicillin using carbon dots anchored on rod-like $CoFe_2O_4$. Chin J Chem Eng 52:136–145. https://doi.org/10.1016/j.cjche.2021.10.030
Shi W, Hao C, Shi Y, Guo F, Tang Y (2023) Effect of different carbon dots positions on the transfer of photo-induced charges in type I heterojunction for significantly enhanced photocatalytic activity. Sep Purif Technol 304:122337. https://doi.org/10.1016/j.seppur.2022.122337
Song G, Deng R, Yao Z, Chen H, Romero C, Lowe T, Driscoll G, Kreglow B, Schobert H, Baltrusaitis J (2020) Anthracite coal-based activated carbon for elemental Hg adsorption in simulated flue gas: preparation and evaluation. Fuel 275:117921. https://doi.org/10.1016/j.fuel.2020.117921
Su L, Chen M, Zhuo G, Ji R, Wang S, Zhang L, Zhang M, Li H (2021) Comparison of biochar materials derived from coconut husks and various types of livestock manure, and their potential for use in removal of $H_2S$ from biogas. Sustainability 13:6262. https://doi.org/10.3390/su13116262
Tang T, Wang Z, Guan J (2022) Electronic structure regulation of single-site M-N-C electrocatalysts for carbon dioxide reduction. Acta Phys Chim Sin 39:2208033. https://doi.org/10.3866/PKU.WHXB202208033
Tang T, Duan Z, Baimanov D, Bai X, Liu X, Wang L, Wang Z, Guan J (2023a) Synergy between isolated Fe and Co sites accelerates oxygen evolution. Nano Res 16:2218–2223. https://doi.org/10.1007/s12274-022-5001-3
Tang T, Wang Y, Han J, Zhang Q, Bai X, Niu X, Wang Z, Guan J (2023b) Dual-atom Co-Fe catalysts for oxygen reduction reaction. Chin J Catal 46:48–55. https://doi.org/10.1016/S1872-2067(22)64189-5
Tang T, Wang Z, Guan J (2023c) Structural optimization of carbon-based diatomic catalysts towards advanced electrocatalysis. Coord Chem Rev 492:215288. https://doi.org/10.1016/j.ccr.2023.215288
Tian W et al (2001) Heteroatom (N or N-S)-doping induced layered and honeycomb microstructures of porous carbons for $CO_2$ capture and energy applications. Adv Funct Mater 26(47):8651–8661
Tuerhong T, Kuerban Z (2022) Preparation and characterization of cattle manure-based activated carbon for hydrogen sulfide removal at room temperature. J Environ Chem Eng 10:107177. https://doi.org/10.1016/j.jece.2022.107177
Vakili F, Rashidi A, Taghavi L, Mansouri N (2021) Single-step synthesis of N, S co-doped waste-derived nanoporous carbon sorbent for mercury vapor removal. Environ Sci Pollut Res 28:17265–17274. https://doi.org/10.1007/s11356-020-12075-2
Wang M-X, Huang Z-H, Shimohara T, Kang F, Liang K (2011) NO removal by electrospun porous carbon nanofibers at room temperature. Chem Eng J 170:505–511. https://doi.org/10.1016/j.cej.2011.01.017
Wang J, Yan Z, Liu L, Chen Y, Zhang Z, Wang X (2014) In situ DRIFTS investigation on the SCR of NO with $NH_3$ over $V_2O_5$ catalyst supported by activated semi-coke. Appl Surf Sci 313:660–669. https://doi.org/10.1016/j.apsusc.2014.06.043
Wang M, Guo Z, Huang Z, Kang F (2016) Preparation of porous carbon nanofibers with controllable pore structures for low-concentration NO removal at room temperature. New Carbon Mater 31:277–286. https://doi.org/10.1016/S1872-5805(16)60013-6
Wang T, Wu J, Zhang Y, Liu J, Sui Z, Zhang H, Chen W-Y, Norris P, Pan W-P (2018a) Increasing the chlorine active sites in the micropores of biochar for improved mercury adsorption. Fuel 229:60–67. https://doi.org/10.1016/j.fuel.2018.05.028
Wang Y, Zhou Y, Shen Y, Zhu S (2018b) Pyridinic N: a special group for enhancing direct decomposition reaction of NO over N-doped porous carbon. Microporous Mesoporous Mater 265:98–103. https://doi.org/10.1016/j.micromeso.2018.02.006
Wang A, Chen W, Liu S, Lin W, Tian C (2023a) Layered porous carbon material derived from food residues and its application for elemental mercury adsorption in flue gas. Fuel 335:126876. https://doi.org/10.1016/j.fuel.2022.126876
Wang H, Wu F, Wu L, Guan J, Niu X (2023b) Nanozyme colorimetric sensor array based on monatomic cobalt for the discrimination of sulfur-containing metal salts. J Hazard Mater 456:131643. https://doi.org/10.1016/j.jhazmat.2023.131643
Wu J, Chen W, Chen L, Jiang X (2022) Super-high N-doping promoted formation of sulfur radicals for continuous catalytic oxidation of $H_2S$ over biomass derived activated carbon. J Hazard Mater 424:127648. https://doi.org/10.1016/j.jhazmat.2021.127648
Xu X, Guo Y, Shi R, Chen H, Du Y, Liu B, Zeng Z, Yin Z, Li L (2021) Natural Honeycomb-like structure cork carbon with hierarchical micro-mesopores and N-containing functional groups for VOCs adsorption. Appl Surf Sci 565:150550. https://doi.org/10.1016/j.apsusc.2021.150550
Xue Y, Guo Y, Zhang Z, Guo Y, Wang Y, Lu G (2008) The role of surface properties of activated carbon in the catalytic reduction of NO by carbon. Appl Surf Sci 255:2591–2595. https://doi.org/10.1016/j.apsusc.2008.07.167
Yang W, Liu Z, Xu W, Liu Y (2018) Removal of elemental mercury from flue gas using sargassum chars modified by $NH_4Br$ reagent. Fuel 214:196–206. https://doi.org/10.1016/j.fuel.2017.11.004
Yang W, Li Y, Shi S, Chen H, Shan Y, Liu Y (2019) Mercury removal from flue gas by magnetic iron-copper oxide modified porous char derived from biomass materials. Fuel 256:115977. https://doi.org/10.1016/j.fuel.2019.115977
Yang C, Florent M, de Falco G, Fan H, Bandosz TJ (2020a) $ZnFe_2O_4$/activated carbon as a regenerable adsorbent for catalytic removal of $H_2S$ from air at room temperature. Chem Eng J 394:124906. https://doi.org/10.1016/j.cej.2020.124906
Yang C, Wang Y, Fan H, de Falco G, Yang S, Shangguan J, Bandosz TJ (2020b) Bifunctional ZnO-MgO/activated carbon adsorbents boost H2S room temperature adsorption and catalytic oxidation. Appl Catal B Environ 266:118674. https://doi.org/10.1016/j.apcatb.2020.118674
Yang M, Wang H, Jin S, Zhang R, Wang Y, Huo W, Wang X, Jin M, Qiao W, Ling L (2021) Insight into the mechanism of boron-doping of carbon aerogel for enhancing the activity of low-temperature selective catalytic reduction of NO with $NH_3$. Catal Sci Technol 11:2057–2072. https://doi.org/10.1039/D0CY02006K
Yao L, Liu Q, Mossin S, Nielsen D, Kong M, Jiang L, Yang J, Ren S, Wen J (2020) Promotional effects of nitrogen doping on catalytic performance over manganese-containing semi-coke catalysts for the $NH_3$-SCR at low temperatures. J Hazard Mater 387:121704. https://doi.org/10.1016/j.jhazmat.2019.121704
Zhang Z, Wang J, Li W, Wang M, Qiao W, Long D, Ling L (2016) Millimeter-sized mesoporous carbon spheres for highly efficient catalytic oxidation of hydrogen sulfide at room temperature. Carbon 96:608–615. https://doi.org/10.1016/j.carbon.2015.10.001
Zhang X, Gao B, Creamer AE, Cao C, Li Y (2017) Adsorption of VOCs onto engineered carbon materials: a review. J Hazard Mater 338:102–123. https://doi.org/10.1016/j.jhazmat.2017.05.013
Zhang X, Ren K, Wang Y, Shen B, Shen F, Shang Y (2021) Solvent-free synthesis of MnOx-FeOx/biochar for Hg $^0$ and *o* -xylene

removal from flue gas. Energy Fuels 35:15969–15977. https://doi.org/10.1021/acs.energyfuels.1c02508

Zhou K, Ma W, Zeng Z, Ma X, Xu X, Guo Y, Li H, Li L (2019) Experimental and DFT study on the adsorption of VOCs on activated carbon/metal oxides composites. Chem Eng J 372:1122–1133. https://doi.org/10.1016/j.cej.2019.04.218

Zhou M, Xu Y, Luo G, Zhang Q, Du L, Cui X, Li Z (2022a) Facile synthesis of phosphorus-doped porous biochars for efficient removal of elemental mercury from coal combustion flue gas. Chem Eng J 432:134440. https://doi.org/10.1016/j.cej.2021.134440

Zhou Q, Di G, Song T, Lu P, Xu G (2022b) Template synthesis of sulfur-doped mesoporous carbon for efficiently removing gas-phase elemental mercury from flue gas. Fuel 321:124112. https://doi.org/10.1016/j.fuel.2022.124112

Zhu Z, Liu Z, Liu S, Niu H (1999) A novel carbon-supported vanadium oxide catalyst for NO reduction with $NH_3$ at low temperatures. Appl Catal B Environ 23:L229–L233. https://doi.org/10.1016/S0926-3373(99)00085-5

Zhu L, Huang B, Wang W, Wei Z, Ye D (2011) Low-temperature SCR of NO with $NH_3$ over $CeO_2$ supported on modified activated carbon fibers. Catal Commun 12:394–398. https://doi.org/10.1016/j.catcom.2010.10.028

Zhu X, Zhang L, Zhang M, Ma C (2019) Effect of N-doping on $NO_2$ adsorption and reduction over activated carbon: an experimental and computational study. Fuel 258:116109. https://doi.org/10.1016/j.fuel.2019.116109